THE JOURNAL OF PHYSICAL CHEMISTRY C

Article

pubs.acs.org/JPCC

Apparent Absorption Spectra of Silica Supported Vanadium−Titanium Oxide Catalysts: Experimental Study and Modeling

S. Klokishner,*[,†] O. Reu,[†] G. Tzolova-Müller,[‡] R. Schlögl,[‡] and A. Trunschke[‡]

[†]Institute of Applied Physics, Academy of Sciences of Moldova, Academy Street 5, MD 2028 Chisinau, Moldova

[‡]Fritz-Haber-Institut der Max-Planck-Gesellschaft, Faradayweg 4-6,14195 Berlin, Germany

ABSTRACT: The structures of different titania, vanadia, and vanadia−titania clusters located on the surface of mesoporous silica SBA-15 are optimized using density functional theory (DFT). The apparent absorption spectra arising from these clusters are calculated with the aid of the ORCA package. The silica support is shown to contribute to the absorption spectra at wavelengths much shorter than those observed for vanadia and titania clusters located on the SBA-15 surface. The comparison of calculated and experimental apparent absorption spectra of supported vanadia and titania catalysts reveals that titania species generally show a higher nuclearity compared to vanadia species at similar low loadings. SBA-15 based catalysts loaded with both vanadia and titania are supposed to contain two types of species: species in which the V ions are anchored to the titania ones and those in which V and Ti ions alternate and are mainly coupled to the support through M−O−Si (M = V, Ti) bridges. The latter provide the major contribution to the apparent absorption spectra at not very high Ti loadings.

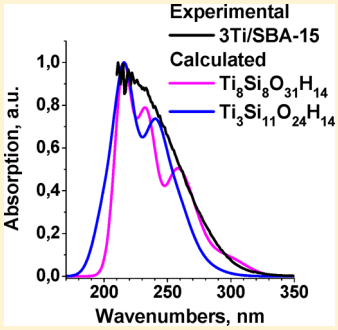

1. INTRODUCTION

In modern heterogeneous catalysis, vanadium oxide based catalysts constitute a very important class of catalytic materials because of their wide application in chemical industry in various oxidation processes. Silica supported vanadium oxide is used in sulfuric acid production by catalytic oxidation of SO_2 to SO_3.[1] The active phase of the catalyst is a very thin layer of a molten salt composed of vanadium pyrosulfate that becomes liquid at reaction temperature (450−610 °C) due to the addition of alkali promoters. Titania supported vanadium oxide is applied in the catalytic oxidation of *o*-xylene to phthalic anhydride[2] and in the selective catalytic reduction (SCR) of nitrogen oxides (NO_x).[3]

Beyond that, vanadium oxide deposited on the surface of high-surface area oxide supports, such as SiO_2, Al_2O_3, TiO_2, and ZrO_2 has been attracted much attention in research dealing with catalysts for oxidative dehydrogenation of short-chain alkanes to the corresponding olefins.[4] Titania supported on SBA-15 has been investigated as catalyst for photocatalytic CO_2 reduction.[5] The molecular structure of vanadium oxide species on these supports has been analyzed by a wide variety of spectroscopic techniques, including Raman, ^{51}V NMR, UV−vis−NIR, and extended X-ray photoelectron spectroscopy.[6−21] The structure of titanium oxide species supported on amorphous silica was investigated as well.[22−29]

Experimental studies show a strong dependence of the reactivity of supported vanadium oxide catalysts in oxidation reactions on the nature of the support,[14,30−32] but the origin of the support effect as well as the reaction mechanisms in selective oxidation are still a subject of debate. The relations between the structure of vanadium oxide species deposited on the surface of the SiO_2, Al_2O_3, TiO_2, and ZrO_2 supports and their reactivity in selective oxidation reactions has been discussed in several reviews.[19,30,31,33−37]

Recently SBA-15,[38,39] an ordered mesoporous silica, has attracted great attention in the field of catalysis. Detailed studies of the effect of vanadium content on the nature of the VO_x species anchored on the surface of SBA-15 show that the high dispersion of vanadium oxide species, the large pore diameter of the support, and the relatively low surface acidity of the catalyst are considered to be responsible for the superior catalytic behavior of VO_x/SBA-15 catalysts in the oxidative dehydration of propane.[40−42] A controlled and reproducible synthesis of SBA-15 supported vanadia catalysts containing between 0.6 and 13.6 vanadium atoms per nm^2 was performed with the use of an ion exchange technique,[41] and a comprehensive structural characterization of these catalysts by nitrogen adsorption, XRD, SEM, TEM, Raman, IR, and UV−vis spectroscopy was reported. The structural similarity of the low-loaded catalysts was shown to be reflected in their Raman spectra and alike catalytic activity during the oxidative dehydrogenation of propane between 380 and 480 °C. Comprehensive experimental studies[40,41] of VO_x/SBA catalysts has demonstrated that the vanadium species anchored to the surface of these catalysts show structural properties similar to those on mesoporous VO_x/MCM-41 and conventional VO_x/SiO_2 catalysts, but a higher surface concentration of isolated and oligomeric VO_x species (i.e., a higher concentration of highly dispersed vanadium oxide species) could be achieved on the surface of SBA-15.

Received: May 2, 2014
Revised: June 6, 2014
Published: June 11, 2014

   dx.doi.org/10.1021/jp504309w | *J. Phys. Chem. C* 2014, 118, 14677−14691

Addressing the support effect, the abundance of Ti−O ligands on the reactivity of silica supported vanadium oxo species in oxidative dehydrogenation of propane was investigated.[42] The topology of the catalyst surface was varied by sequential grafting of titanium and vanadium alkoxides generating an extended library of mixed $(VO_x)_n-(TiO_x)_n$/SBA-15 catalysts. Segregation of nanocrystalline vanadia and titania particles was excluded by UV−vis, Raman, and NEXAFS spectroscopy. Monolayer coverage of titanium oxide surface species has been achieved in the range between 17 and 19 wt % Ti loading corresponding to 6−8 Ti atoms per nm^2 and Si/Ti ratios between 3.3 and 2.8. At low titania loadings, vanadia is grafted on both the silica surface and surface titania species yielding tetrahedrally coordinated vanadium oxo species characterized by low nuclearity and moderate catalytic activity. A maximum in the catalytic activity has been achieved at a critical total metal loading that corresponds to a VO_x-TiO_x monolayer in which the vanadium oxide species appear to be embedded in between TiO_x surface species forming a joint monolayer, but not a bilayer.

Although progress has been made in recent years in characterization of vanadium oxide supported on SiO_2 (including MCM-41 and SBA-15), Al_2O_3, TiO_2, and ZrO_2 under different environments through spectroscopic studies, there still remain many unresolved questions that need to be addressed. First of all is the identification of vanadium species present on the support, the structure of which strongly depends on the type of the support, the loading, the degree of hydration, etc. An overview of different models describing the structure of the active VO_x species on top of the supporting material is given by Muylaert et al.[36] and van Lingen et al.[43] There is a consensus that under dehydrated conditions the monomeric structure present at low loadings is a distorted tetrahedron around the central vanadium atom containing one V═O bond. There is still no agreement on the precise molecular structure of this species. Four different possibilities have been discussed in the literature for the way the monomeric VO_4 species is anchored at the support after dehydration: (a) The classical pyramid model, introduced in the 1980s, with three Si−O−V bonds connecting it to the surface of the support and a mono-oxo V═O on top (Scheme 1a), is the most acknowledged.[44−47] The single V═O nature of the VO_4 unit has been confirmed with ^{18}O labeling experiments[48,49] and Raman spectroscopic analysis.[50] (b) Species with two Si−O−V support bonds, a V═O, and a V−OH group[51−55] (Scheme 1b). (c) The model in which two V−O−Si bonds are replaced by two OH groups giving a structure with one bond to the support[56] (Scheme 1c). (d) The umbrella model[56−58] that considers a species containing a vanadium atom linked to the surface via only one Si−O−V bond, one V═O bond, and a perturbed O_2 molecule linked to the central vanadium atom (Scheme 1d). At the same time, recent EXAFS measurements and IR and Raman spectroscopic studies on low-loaded supported vanadium oxide species on aluminia, silica, niobia, and zirconia performed under almost identical conditions[56,59] reveal the presence of V−OH groups, thus giving the support for either structure (b) or structure (c).[36] X-ray absorption fine structure near the O K-edge (NEXAFS) was revealed to be a sensitive spectroscopic technique that allows in combination with DFT calculations the analysis of the molecular structure of silica supported vanadium oxide species in the presence of ambient gas phase oxygen.[60] This technique was applied in 0.5 mbar of O_2 at 400 °C to V_xO_y/SBA-15 catalysts containing 2.7 and 10 wt % vanadium,

Scheme 1. Schematic Representation of Monomeric Vanadia Species[a]

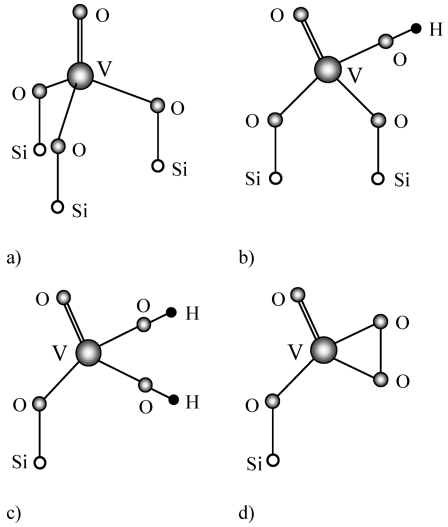

[a](a) V═O(OSi)$_3$; (b) V═O(OH)(OSi)$_2$; (c) V═O(OH)$_2$(OSi); (d) V═O(O)$_2$(OSi) suggested to be present at the surface of silica supports.

respectively.[61] It was obtained that the exclusive presence of monomeric vanadium oxide species at the surface of silica can be ruled out even at low loadings. Both catalysts contain a mixture of monomeric and oligomeric vanadium oxide species. Recent resonant Raman spectroscopy studies with different excitation-laser wavelengths point to the presence of three different monomeric VO_4 species on alumina at a loading as low as 0.16 V/nm^2.[21,62] Multiwavelength Raman and in situ UV−vis studies[63] of the molecular structure of silica supported vanadium oxide catalysts over a wide range of surface VO_x density (0.0002−8 V/nm^2) have shown that three major Raman bands at 920, 1032, and 1060 cm^{-1} observed on dehydrated samples can be mainly associated with symmetric V−O−Si, V═O, and antisymmetric V−O−Si modes, respectively. At least two different monomeric vanadia species have been identified coexisting on highly dehydrated silica surfaces in an extremely wide VO_x loading range. The authors arrived at the conclusion that one of the two monomeric species has pyramidal structure and the other is in the partially hydroxylated pyramidal mode.[63]

The issue of the molecular structure of metal oxide surface species in supported vanadia and titania catalysts has been discussed in several theoretical studies. In the early work by Kobayashi et al., ab initio Hartree−Fock molecular-orbital method has been used to investigate the electronic structure of a VO_4H_3 cluster as a model for silica supported vanadium oxide catalysts.[64] Ab initio molecular orbital calculations performed in ref 65 have confirmed the tetrahedral $(V═O)O_3$ structure of vanadium species in low-loaded V_2O_5/SiO_2 catalyst proposed on the basis of UV−vis spectroscopy, Raman spectroscopy, XANES, EXAFS, and XPS. A systematic study combining infrared absorption and Raman spectroscopic measurements with DFT calculations for model compounds and surface models for both the vanadia/silica and the vanadia/aluminia system have been performed by Magg et al.[66] Van Lingen et al. calculated the infrared and Raman spectra for the above-mentioned monomeric species (a)−(c) anchored to the catalyst surface.[43] It was concluded that the presence of a particular

dx.doi.org/10.1021/jp504309w | J. Phys. Chem. C 2014, 118, 14677−14691

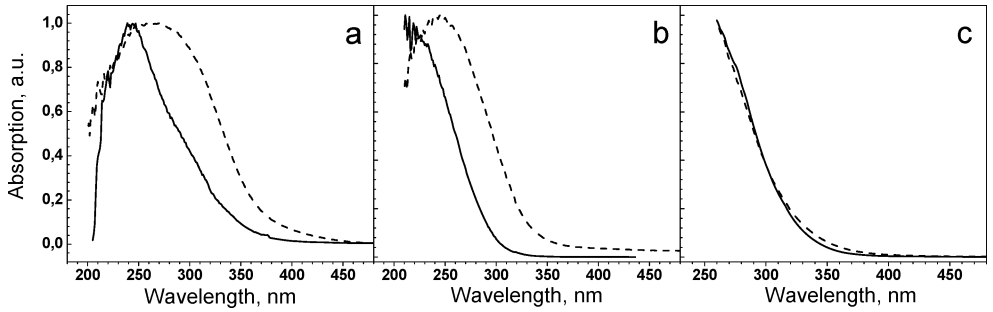

Figure 1. Observed UV−vis spectra of selected VO_x/SBA-15, TiO_x/SBA-15, and VO_x−TiO_x/SBA-15 catalysts after dehydration in flowing synthetic air at 450 °C for a period of 1 h. Solid lines: 1V/SBA-15 (a), 3Ti/SBA-15 (b), 4V3Ti/SBA-15 (c). Dashed lines: 4V/SBA-15 (a), 8Ti/SBA-15 (b), 4V8Ti/SBA-15 (c).

species depends on the method of preparation of the compound, and two models, the umbrella model and the model with two bonds to the support, described the actual systems best. Furthermore, DFT was applied to molecular and embedded cluster models for vanadia on three different crystalline silica supports (edingtonite, hexagonal prism slab, cristobalite) that span the range of local structures found in amorphous silica.[67] The assignment of the vibrational modes for monomeric, dimeric, and polymeric sites has been fulfilled. In order to analyze structural details of the vanadia species on the surface of SBA-15, DFT calculations on oxygen core excitations in vanadia-silica model clusters were combined with in situ NEXAFS measurements near the oxygen K-edge.[61] It was shown that differently coordinated oxygen atoms can be identified in the O K-NEXAFS spectrum by comparison with theoretical spectra obtained by state of the art DFT calculation.

The 1s core excitation spectra of clusters simulating local sections of anatase TiO_2 bulk and of silica supported titania model clusters have been evaluated using DFT cluster methods.[29] It was found that the experimental spectra are reproduced quite nicely examining clusters that include Ti−O bonds, Ti−O−Si bridges characterizing titania−support binding, and Ti−O−H bridges involving OH groups. Clusters including double-bonded titanyl oxygen species do not contribute to the observed NEXAFS spectra.

Vanadia, titania, and vanadia/titania catalysts supported on mesoporous silica SBA-15 are complex materials, and the identification of the molecular structure of the surface species by complementary experimental methods is an important task that contributes to a better understanding of catalysts' performance. Important information about the intrinsic structure of the catalyst can be provided by UV−vis spectroscopy that represents one of the methods of identification and quantitative estimation of different types of supported species. To our knowledge no attempts at a quantitative analysis of the optical spectra of vanadia, titania, and vanadia/titania species located on SBA-15 have been undertaken until now. Thus, the aim of the present study is to model the UV−vis spectra of these species. At the first step on the basis of qualitative considerations and results obtained in preceding papers we will select and optimize the structure of the potential species, which may be responsible for the observed UV−vis bands. The second step will contain the calculation of the spectra arising from the selected species and estimation on this basis of their possible contributions to the observed spectra. This step actually represents a testing of the adequacy of the model to observations. At the last stage we shall attempt to explain the observed spectra peculiarities and show which information concerning the composition of vanadia and titania species anchored to the support can be extracted from the analysis of these spectra.

The paper is organized as follows: in section 2 we describe the observed apparent absorption spectra and discuss qualitatively the red shift of the bands with increase of the nuclearity of V and Ti clusters anchored to the support. In section 3 we describe the computational details, and in section 4 the cluster models are presented. The shapes of the optical bands arising from different vanadia, titania, and vanadia−titania clusters deposited on the catalyst surface are discussed in section 5. Here we also compare the calculated spectra of the clusters with the observed spectra of the catalysts. On this basis we reveal which clusters are active in the apparent absorption of the catalysts. The conclusions are given in section 6.

2. EXPERIMENTAL DETAILS AND RESULTS. QUALITATIVE DISCUSSION

The UV−vis apparent absorption spectra of 3Ti/SBA-15 (3 wt % Ti loading (sample ID 7676)), 8Ti/SBA-15 (8 wt % Ti loading (sample ID 7731)), 1V/SBA-15 (1 wt % V loading (sample ID 7779)), 4V/SBA-15 (4 wt % V loading (sample ID 7815)), 4V3Ti/SBA-15 (4 wt % V and 3 wt % Ti loading (sample ID 7620)), and 4V8Ti/SBA-15(4 wt % V and 8 wt % Ti loading (sample ID 7624)) in the range between 200 nm (50000 cm^{-1}) and 500 nm (20000 cm^{-1}) (Figure 1) were taken at room temperature with a Perkin Elmer Lambda 650 instrument equipped with an in situ cell (Harrick Praying Mantis diffuse reflectance attachment DRP-P72 in combination with a HVC-VUV reaction chamber). The dehydrated SBA-15 was used as the white standard. To ensure good spectral quality, the maximum value of Kubelka−Munk function $F(R)$ was kept below 1 by diluting the sample 20-fold with the SBA-15 white standard. Spectra were measured before and after the mixtures were heated to 450 °C, allowed to dry under a stream of synthetic air for 1 h, and cooled to room temperature again.

According to XPS (data not shown), the valence states of vanadium and titanium ions in VO_x/SBA-15 and TiO_x/SBA-15 after this treatment are pentavalent and tetravalent, respectively. The UV−vis apparent absorption spectra of 3Ti/SBA-15, 8Ti/SBA-15, 1V/SBA-15, 4V/SBA-15, 4V3Ti/SBA-15, and 4V8Ti/SBA-15 in the range between 25000 and 50000 cm^{-1} are assigned to electron transfer from oxygen orbitals to titanium and vanadium 3d orbitals, respectively. The following considerations also testify this assignment. For many transition metal ions a strong overlap of the d−d and LMCT bands is observed, which complicates the discrimination of these bands. The situation is quite different for tetrahedrally coordinated V^{4+}

dx.doi.org/10.1021/jp504309w | J. Phys. Chem. C 2014, 118, 14677−14691

and Ti^{3+} ions.[42] Due to the single d-electron, these ions possess a rather simple ligand field diagram with a comparatively small energy gap between the ground $^2E(e^1)$ and the excited $^2T_2(t_2^1)$ states, and, therefore, their ligand-to-metal charge transfer bands are well separated from the less intense d−d bands. The obtained apparent absorption spectra (Figure 1) do not show any optical bands at wavelengths $\lambda > 400$ nm (<25.000 cm^{-1}), and, consequently, the presence of V^{4+} and Ti^{3+} ions can be excluded.

Briefly surveying the experimental data on the apparent absorption spectra of dehydrated VO_x/SBA-15, TiO_x/SBA-15, and VO_x−TiO_x/SBA-15 catalysts in the case of low V and Ti loadings (Figure 1), we can demonstrate the following features:

(i) The widths and the shapes of the bands corresponding to 1 and 4 wt % V on SBA-15 differ in the range between 250 and 400 nm (40000−25000 cm^{-1}). The maximum of the band at 4 wt % of V is shifted to lower energies as compared to that of the band at 1 wt %; this shift is non-negligible and amounts to 3080 cm^{-1} = 0.38 eV. A band, which shows absorption features between 220 and 580 nm, which would indicate the presence of crystalline vanadium pentoxide, has not been found in the UV−vis spectra, even not for samples with the higher vanadium loading.[42]

Within this series of catalysts, the degree of polymerization increases with increasing loading from 1 to 9 wt % of V,[42] which is reflected in the shift of the absorption maximum from 245 nm (40816 cm^{-1}) to 295 nm (33898 cm^{-1}). Along with the findings of other authors,[21,36,43−56,59,62,63] this observation allows one to assume that species of low vanadia nuclearity contribute to the spectra with 1 and 4 wt % of V, respectively.

(ii) A pronounced change in the position and shape of the charge transfer band is observed when passing from the sample with 3 wt % of Ti to that with 8 wt % of Ti. Since the oxidation state of titania is lower than that of vanadia, the band arising from the electron transfer in a single O^{2-}−Ti^{4+} pair is characterized by higher energy than that arising from the transfer in the O^{2-}−V^{5+} pair. Accordingly, the spectra corresponding to 1−4 wt % of V and 3−8 wt % of Ti approximately fall into the same range of wavelengths. From this it is plausible to conclude that the nuclearity of titania species in samples with 3−8 wt % of Ti is higher than that of vanadia ones in samples with 1−4 wt % of V.

(iii) The coincidence of the observed bands of samples 4V3Ti/SBA-15 and 4V8Ti/SBA-15 speaks in favor of the assumption that the spectra of these samples are mainly determined by the V^{5+}−O^{2-} charge transfer bands.

(iv) Finally, the following simple qualitative considerations illustrate the red shift of the observed charge transfer bands with the increase of vanadia or titania content: Let us consider linear binuclear, trinuclear, tetranuclear, and pentanuclear vanadia species (Figure 2). Under action of light the electron jumps from the oxygen ligand to a vanadium ion. If the positions of all vanadium ions in the species are equivalent (similar nearest oxygen environment, see Figures 2a−2d), there is a possibility for the electron to migrate between the neighboring vanadium ions. For all clusters depicted in Figures 2a−2d the transfer parameter p can be taken approximately equal since electron transfer occurs between neighboring ions

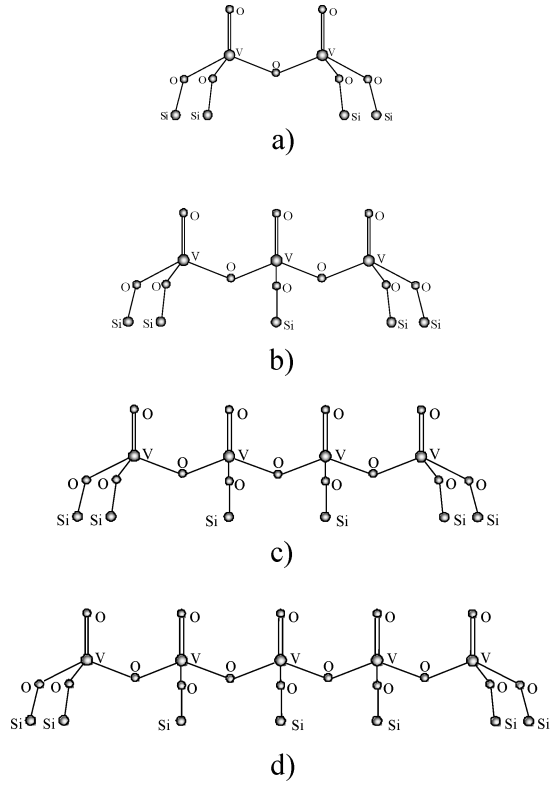

Figure 2. Schematic presentation of the molecular structure of polynuclear vanadia species on silica support.

mediated by the same bridges. Due to electron tunneling the d-orbital in a binuclear species splits into two orbitals (Figure 3a), and two charge transfer bands at $\Delta + p$ and

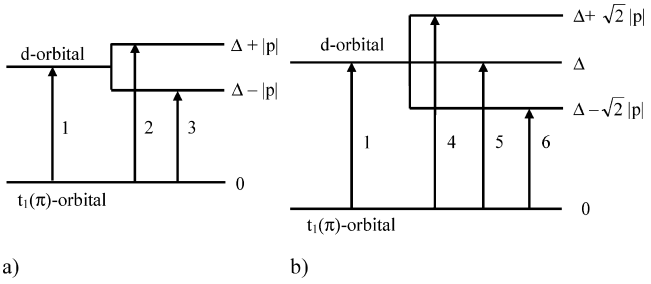

Figure 3. Schematic illustration of the red shift of the absorption spectra for binuclear species (a) and trinuclear species (b): 1, charge transfer band of a single V ion; 2, 3, charge transfer bands for binuclear species; 4, 5, 6, charge transfer bands for trinuclear species.

$\Delta - p$ appear instead of one. In the trinuclear species (Figure 3b) the d-orbital splits into three orbitals with the energies $\Delta - p\sqrt{2}$, Δ, and $\Delta + p\sqrt{2}$. Thus, the lowest in energy charge transfer band will be at $\Delta - p\sqrt{2}$. One can easily see that the lowest in energy charge transfer band shifts to the red by $(\sqrt{2} - 1)|p|$ when passing from a binuclear species (Figure 2a) to a trinuclear one (Figure 2b). A more pronounced shift to the red of the lowest in energy charge transfer band (as compared with binuclear species) is obtained for tetranuclear and pentanuclear species. In these cases the lowest in energy bands shift to the red by $(0.5\sqrt{5} - 1)|p|$ and $(\sqrt{3} - 1)|p|$, respectively. In reality the picture is much more complicated since the interaction with the

dx.doi.org/10.1021/jp504309w | J. Phys. Chem. C 2014, 118, 14677−14691

vibrations of the nearest environment should be taken into account. However, this simple qualitative illustration gives the possibility to understand why the charge transfer band shifts to the red with the increase of the vanadium content in V/SBA-15. The same explanation is valid for Ti/SBA-15. At the same time this explanation does not take into account the interaction of the V and Ti ions with the vibrations of the nearest environment playing a crucial role for the determination of the positions, shapes, and number of the charge transfer bands. Finally, it should be also mentioned that for mixed V−Ti species the electron transfer between V and Ti ions is aggravated by the difference in the ionization potentials, and the simple picture presented in Figure 3 is not relevant. Further on we apply the DFT method to the optimization of the structure of species and calculation of the profiles of the absorption bands.

3. COMPUTATIONAL DETAILS

The optimization of the structure of the clusters assumed to be responsible for the apparent absorption spectra of VO_x/SBA-15, TiO_x/SBA-15, and VO_x−TiO_x/SBA-15 catalysts as well as the calculation of their spectra have been performed within the frames of density functional theory (DFT)[68] using the program package ORCA 2.8.[69,70] In our work we have employed the gradient corrected revised Perdew−Burke−Ernzerhof (RE-VPBE) functional as the hybrid functional. Representative references for the REVPBE functional one can find in the literature.[71−77] The calculations were performed using the Ahlrichs-TZV basis functions[78] as well as their "def2" variants[79] developed more recently. Calculations labeled RIJCOSX[80] used the COSX approximation for the exchange terms in conjunction with the RI-J approximation. The TDDFT method within the ORCA package was applied to calculate the excited state energies, gradients, and equilibrium geometries of the examined clusters. It should be underlined that the excitation energies have been computed with REVPBE optimized geometries. The ground-state energy and density were converged to 10^{-8} au and 10^{-7} au, respectively (ORCA keyword TightSCF). The ORCA program also provided the values of adiabatic minima transition energies calculated as differences between the excited- and ground-state energies in their equilibrium structures.

4. CLUSTER MODELS

In the present calculations we employ model titania−silica, vanadia−silica, and (titania−vanadia)−silica clusters whose initial structures were obtained from chemical reasoning or previously suggested in the literature. We assume that in the clusters, which will be examined, the vanadia and titania ions are arranged in different ways and bound to the support through the bridges: Ti−O−Si, V−O−Si, and V−O−Ti−O−Si. Based on the oxidation states (+4) and (+5) as determined by XPS for Ti and V, respectively, we also suppose that the nearest oxygen environment of the ions is tetrahedral. For titania species with four Ti−O bonds and V species with three V−O bonds and one V═O bond the number of M−O−Si (M = V, Ti) bridges to the support can vary between 1 and 3. In addition, bonds of the type M−OH can be present in the species. Besides this, for silica supported vanadia the umbrella model[56−58] will be also examined. The geometrical structure of the species to be considered are derived from the polyhedral oligometalla silsesquioxanes (POMSS) obtained in ref 81 with the aim to use POMSS as models for silica supported V, Ti, and V/Ti catalysts. The $Si_8O_{12}H_8$ molecule (Figure 4) is of cubic

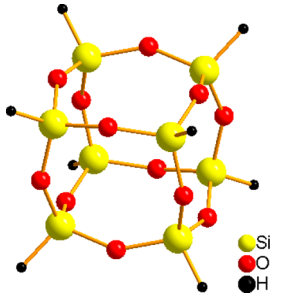

Figure 4. Optimized geometric structure of the model cluster representing the silica support.

structure with silicon occupying the corners and oxygen near the edge midpoints, while hydrogen saturates the dangling bonds at the silicon corners. The structure of this molecule presented in Figure 4 has been optimized using the ORCA package.[69,70] Titania, vanadia, or titania−vanadia species were added to the $Si_8O_{12}H_8$ molecule or to several of these molecules, in order to obtain titania−silica, vanadia−silica, (titania, vanadia)−silica model clusters, which are also optimized with respect to their geometry at the DFT level, including all atoms of the cluster (see below).

The optimized structures for titanium clusters obtained using the ORCA package[69,70] are depicted in Figure 5. In all clusters the titanium ion is in a tetrahedral oxygen environment. The following clusters have been examined: (a) TiOH−$Si_7O_{12}H_7$ ($TiSi_7O_{13}H_8$), (b) $Ti(OH)_2$−$Si_7O_{12}H_8$ ($TiSi_7O_{14}H_{10}$), (c) $(TiOH)_2$−$Si_6O_{12}H_6$ ($Ti_2Si_6O_{14}H_8$), (d) $(TiOH)_3$−$Si_5O_{12}H_5$ ($Ti_3Si_5O_{15}H_8$), (e) $(TiOH)_4$−$Si_4O_{12}H_4$ ($Ti_4Si_4O_{16}H_8$), (f) $(TiOH)_4$−$Si_4O_{12}H_4$ ($Ti_4Si_4O_{16}H_8$), (g) $(TiOH)_2$−$Si_{12}O_{21}H_{12}$ ($Ti_2Si_{12}O_{23}H_{14}$), (h) $(TiOH)_3$−$Si_{11}O_{21}H_{11}$ ($Ti_3Si_{11}O_{24}H_{14}$), (i) $Si_7O_{12}H_7Ti$−O−$TiSi_7O_{12}H_7$ ($Ti_2Si_{14}O_{25}H_{14}$), (j) $Si_4O_{12}H_4(TiOH)_3Ti$−O−$Ti(TiOH)_3Si_4O_{12}H_4$ ($Ti_8Si_8O_{31}H_{14}$). Figures 5a and 5b represent mononuclear titania species, while two titanium ions are contained in clusters (c), (g), and (i). Trinuclear Ti clusters are presented in Figures 5d and 5h. In the cluster (e) (Figure 5e), the titanium ions form a tetragon, while the structure in Figure 5f has a tetrahedral shape. Two tetrahedra-like species are connected in cluster (j). Species (a) couples with the silica support by three Ti−O−Si bridges, while species (b) is bound by two Ti−O−Si bridges. In species (c), (e), and (g) the number of Ti−O−Si bonds corresponds to four, while in species (d) and (h) one can observe five Ti−O−Si bonds. The number of Ti−O−Si bridges in clusters (i) and (f) is six. Cluster (j) is characterized by 12 Ti−O−Si bridges. It should be mentioned that the composition of species (a), (c), (d), (e), and (g)−(j) has been suggested by the authors of the present work, while that of species (b) and (f) was taken from the literature.[29] The optimization of the structure of all species shown in Figure 5 has been performed in the present work with the aid of the ORCA package.

The composition of vanadia species (a), (c)−(h), and (j) (Figure 6), i.e., the number of O, Si, and V atoms and their mutual arrangement, has been taken from the literature.[57,58,61] The optimization of the structure of these species has been performed using the input X-ray data for silsesquioxane $Si_8O_{12}H_8$.[81] The structure of complexes (b) and (i) was

dx.doi.org/10.1021/jp504309w | J. Phys. Chem. C 2014, 118, 14677−14691

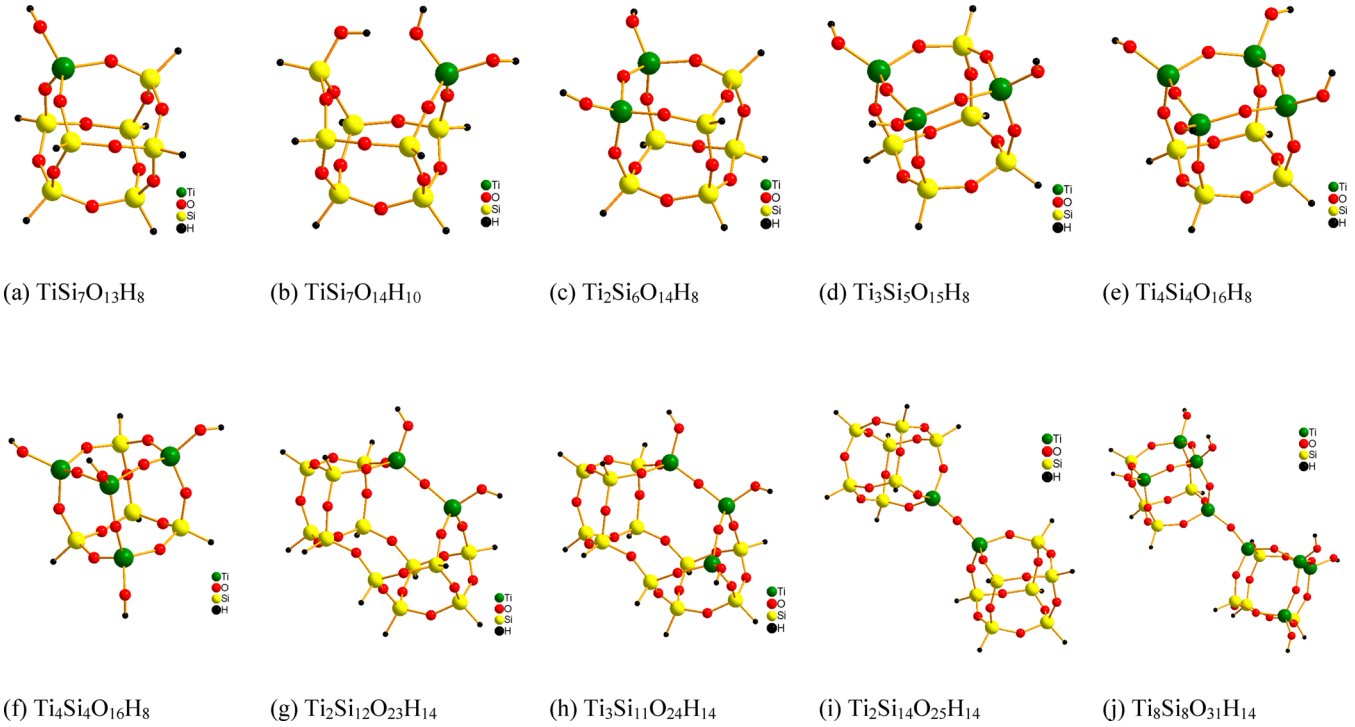

(a) $TiSi_7O_{13}H_8$ (b) $TiSi_7O_{14}H_{10}$ (c) $Ti_2Si_6O_{14}H_8$ (d) $Ti_3Si_5O_{15}H_8$ (e) $Ti_4Si_4O_{16}H_8$

(f) $Ti_4Si_4O_{16}H_8$ (g) $Ti_2Si_{12}O_{23}H_{14}$ (h) $Ti_3Si_{11}O_{24}H_{14}$ (i) $Ti_2Si_{14}O_{25}H_{14}$ (j) $Ti_8Si_8O_{31}H_{14}$

Figure 5. Geometric structures of titania−silica model clusters. The ball-and-stick models show clusters for Ti in tetrahedral coordination with Ti−O−Si and Ti−O−H bond bridges. The composition of each cluster is given below its picture.

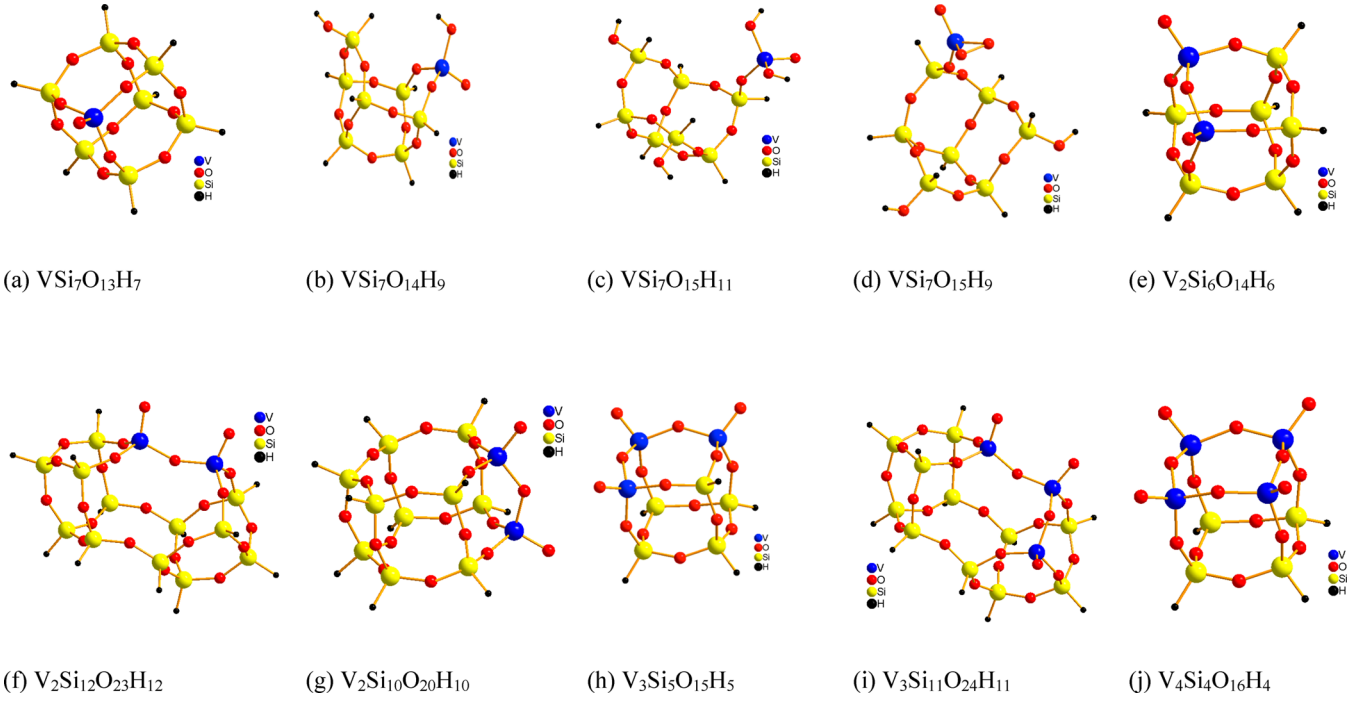

(a) $VSi_7O_{13}H_7$ (b) $VSi_7O_{14}H_9$ (c) $VSi_7O_{15}H_{11}$ (d) $VSi_7O_{15}H_9$ (e) $V_2Si_6O_{14}H_6$

(f) $V_2Si_{12}O_{23}H_{12}$ (g) $V_2Si_{10}O_{20}H_{10}$ (h) $V_3Si_5O_{15}H_5$ (i) $V_3Si_{11}O_{24}H_{11}$ (j) $V_4Si_4O_{16}H_4$

Figure 6. Geometric structures of vanadia−silica model clusters. The ball-and-stick models show clusters for V in tetrahedral coordination with V−O−Si, V−O−H, and V−O_2 bond bridges. The composition of each cluster is given below its picture.

suggested in the present work. Like in the case of titanium it is assumed that vanadium is in a tetrahedral environment. However, as distinguished from titania clusters, the vanadia ones contain a double V═O bond. The final structures of the V clusters obtained from geometry optimizations are shown in Figures 6a−6j. In the monomeric and nonmonomeric clusters, the vanadium atoms present a wide variety of different arrangements. The shapes of the vanadia clusters are the following. The cluster $VSi_7O_{13}H_7$ (Figure 6a), in general, resembles the $Si_8O_{12}H_8$ species (Figure 4), however, one Si−H moiety is replaced by V═O. This cluster contains three V−O−Si bridges with the silica surface. The $VSi_7O_{14}H_9$ cluster (Figure 6b) contains two bonds V−O−Si, a double bond V═O, and a V−OH bond. To obtain the structure of the complex

dx.doi.org/10.1021/jp504309w | J. Phys. Chem. C 2014, 118, 14677−14691

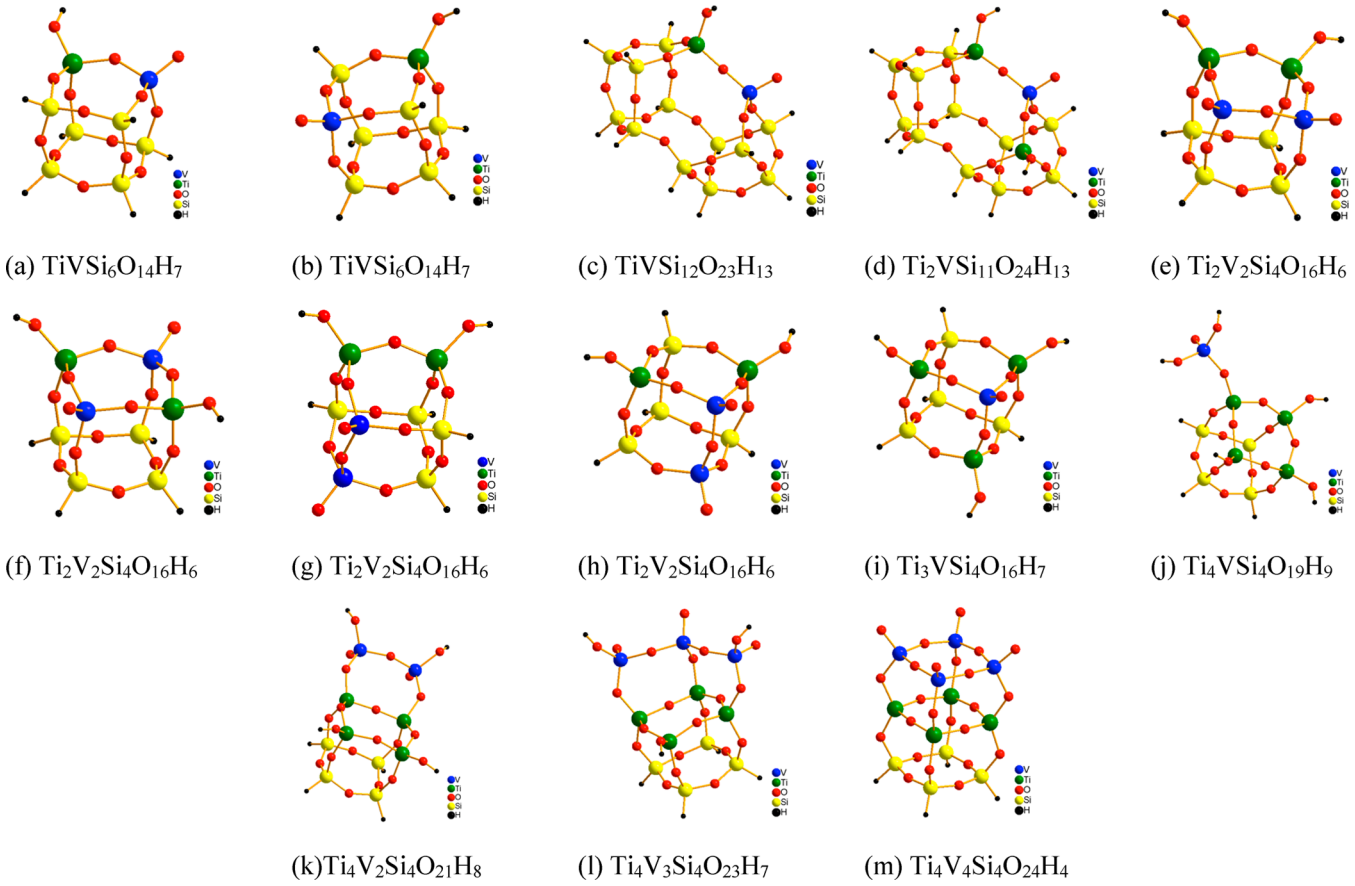

Figure 7. Geometric structures of vanadia−titania−silica model clusters. The ball-and-stick models show clusters for V and Ti in tetrahedral coordination. The composition of each cluster is given below its picture.

$VSi_7O_{15}H_{11}$ (Figure 6c) it is necessary to add two OH ligands to vanadium as well as to connect two silicon atoms with OH groups. In this complex vanadium is bound with the surface by one V−O−Si bridge and represents the so-called umbrella geometry. The cluster $VSi_7O_{15}H_9$ (Figure 6d) is known in the literature as the peroxo species.[57,58,61] The binuclear vanadia species $V_2Si_6O_{14}H_6$, $V_2Si_{12}O_{23}H_{12}$, and $V_2Si_{10}O_{20}H_{10}$ are presented in Figures 6e−6g. The species $V_2Si_6O_{14}H_6$ (Figure 6e) is simply obtained from the $Si_8O_{12}H_8$ species by replacing two Si−H groups by two V═O groups. The structures of clusters $V_2Si_{12}O_{23}H_{12}$ and $V_2Si_{10}O_{20}H_{10}$ (Figures 6f and 6g) actually represent the combination of two broken cubes originating from $Si_8O_{12}H_8$ with the subsequent replacement of Si−H by V═O. Each of these species is linked with the surface of the support by four V−O−Si bridges. The complex $V_3Si_{11}O_{24}H_{11}$ (Figure 6i) has been obtained from $V_2Si_{12}O_{23}H_{12}$ replacing Si−H by V═O. It has five V−O−Si bridges to the support. Finally, the structure of complexes $V_3Si_5O_{15}H_5$ and $V_4Si_4O_{16}H_4$ (Figures 6h and 6j) can be easily obtained from the $V_2Si_6O_{14}H_6$ structure by replacing one or two Si−H groups by the same number of V═O groups. These trinuclear and binuclear vanadia clusters have 5 and 4 V−O−Si bridges to the support, respectively.

In modeling of the mixed V−Ti species (Figure 7) we also base on the structure of the silsesquioxane $Si_8O_{12}H_8$ cluster. Three groups of mixed V−Ti species can be distinguished. In the first group of V−Ti species (Figures 7a−7g) the vanadium and titanium atoms alternate in different ways, but the main feature of these species is that the bonds V−O−Si and Ti−O−Si do exist. The second type of V−Ti species is represented by species which are anchored to the support via V−O−Ti−O−Si bonds (Figures 7 i−7m). Finally, the species (h) (Figure 7h) contains both types of bonds. At the same time in mixed V−Ti catalysts the presence of mononuclear or polynuclear species containing only V or Ti ions is also possible.

Finally, the structure of the $Ti_9O_{30}H_{24}$ cluster (Figure 8) was optimized with the further aim to reproduce the apparent absorption spectrum of the anatase TiO_2 bulk. The Ti_9O_{30} part of this cluster reflects the structure of anatase.

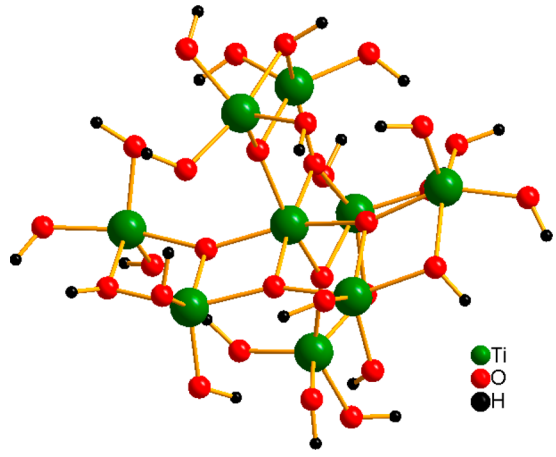

Figure 8. Geometric structure of the model $Ti_9O_{30}H_{24}$ cluster representing the structure of anatase.

dx.doi.org/10.1021/jp504309w | J. Phys. Chem. C 2014, 118, 14677−14691

5. CALCULATION OF THE ABSORPTION SPECTRA OF TiO_x, VO_x, AND MIXED VO_x–TiO_x SPECIES DEPOSITED ON THE SURFACE OF THE SBA-15 SUPPORT. QUALITATIVE DISCUSSION OF THE OBSERVED SPECTRA OF THE CATALYSTS

5.1. Short Overview of Basic Theory in the Field of Optical Spectroscopy of Local Centers. The absorption spectra of the mentioned clusters in fact represent charge transfer bands arising from ligand to metal transitions. The calculations performed at the DFT level testify that the molecular orbitals of all clusters shown in Figures 4–8 are orbitally nondegenerate. Thus, for the description of the ligand to metal charge transfer bands the formula for the absorption coefficient for the band arising from the singlet–singlet transition should be applied. A short excursus to the history of this subject shows that in basic works[82,83] the shape of the band for these transitions was obtained in the single-mode approximation, neglecting the frequency effect and the dispersion of the vibrational mode. In this case, the spectrum represents a set of equidistant absorption lines with the natural line width $\gamma \ll \omega$ spaced by the limit vibrational frequency ω. Later on, this formula, independently obtained by the authors of papers,[82,83] was called "Pekarian".[84] The dispersion of crystal vibrations in the examination of optical spectra of local centers was considered for the first time by Krivoglaz and Pekar[85] who also discovered the zero-phonon line. The most important development and generalization have been performed in ref 86. Using the method of generating function, Kubo and Toyozawa discussed the shape of the absorption band of a trapped electron in insulating or semiconducting crystals,[86] especially its temperature dependence. An ample overview of the state of the art in theory of optical electron-vibrational bands can be found in the review papers 87,88 and monograph 89. Following refs 87,89 the form-function for the absorption band on the singlet–singlet transition s → p of a local center in a crystal looks as follows:

$$F_{sp}(\Omega) = \frac{1}{2\pi}\int_{-\infty}^{\infty} \exp[i(\Omega_{ps} - \Omega)t + f_p(t)]\, dt \tag{1}$$

where

$$f_p(t) = -\frac{1}{2}\sum_{\kappa}\Delta_{\kappa p}^2 \coth\frac{\beta_\kappa}{2} + \frac{1}{2}\sum_{\kappa}\Delta_{\kappa p}^2 \frac{\cos(\omega_\kappa t - i\beta_\kappa/2)}{\sinh\frac{\beta_\kappa}{2}} \tag{2}$$

The indices s and p correspond to the ground and excited electronic states, respectively, $\kappa \equiv \boldsymbol{\kappa}\nu$ stands for the wave vector $\boldsymbol{\kappa}$ of the phonon and ν numbers the branches of crystal vibrations, $\hbar\omega_\kappa$ is the phonon energy, $\beta_\kappa = \hbar\omega_\kappa/kT$, $\hbar\Omega_{ps} = J_p - J_s$,

$$J_i = \langle i|V_\kappa|i\rangle - \sum_{\kappa}\frac{\hbar\omega_\kappa}{2}q_{ki}^{\ 2} \quad (i = p, s) \tag{3}$$

J_i is the adiabatic potential minimum, V_κ is the operator of electron-vibrational interaction, and $q_{ki} = -\langle i|V_\kappa|i\rangle/\hbar\omega_\kappa$ is the equilibrium coordinate of the vibrational subsystem in the electronic state i, $\Delta_{\kappa p} = q_{\kappa p} - q_{\kappa s}$, and finally, Ω is the frequency of light. The absorption coefficient is $K_{sp}(\Omega) \sim \Omega F_{sp}(\Omega)$. In the case of interaction with local vibrations and optical phonons possessing negligibly small dispersion ($\omega_\kappa = \omega_0$) expression 1 for $F(\Omega)$ takes on the form[82,83,87,89]

$$F_{sp}(\Omega) = \exp\left(-\frac{a}{2}\coth\frac{\beta}{2}\right)\sum_{n=-\infty}^{\infty}\exp\left(n\frac{\beta}{2}\right)I_n(z)\delta(\Omega - \Omega_{ps} - n\omega_0),$$
$$z = \frac{a}{2\sinh(\beta/2)}, \quad a = \sum_{\kappa}\Delta_\kappa^2 \tag{4}$$

Here, $I_n(z)$ is the modified Bessel function. Each term of eq 4 describes a δ-type absorption line corresponding to a transition accompanied by generation of n vibrational quanta; the terms with negative n values correspond to the transitions from the excited vibrational sublevels. To take into account the width of the electronic states the shape function $\delta(\Omega - \Omega_{ps} - n\omega_0)$ of each individual line should be replaced by a Gaussian or Lorentz curve, respectively. In the ORCA package[70] the program for calculation of the optical bands is oriented on isolated clusters and based in principle on eq 2, in which the summation over κ is substituted by the summation over the finite number of the vibrational frequencies of an isolated complex.[90] Since the frequencies of the cluster vibrations form a discrete spectrum and do not manifest dispersion to avoid divergences in the form-function $F_{sp}(\Omega)$ (see eq 4) the integrand in the expression 1 for the form-function of the absorption band is presented in the ORCA package as the product of two exponents

$$\exp[i(\Omega_{ps} - \Omega)t + \varphi_p(t)], \quad \exp(-\Gamma_p t - \theta_p^{\ 2}t^2) \tag{5}$$

where $\varphi_p(t)$ (see eq 1 in ref 90) has a form identical to $f_p(t)$

$$\varphi_p(t) = -\frac{1}{2}\sum_{j}\Delta_{jp}^2 \coth\frac{\beta_j}{2} + \frac{1}{2}\sum_{j}\Delta_{jp}^2\frac{\cos(\omega_j t - i\beta_j/2)}{\sinh\frac{\beta_j}{2}} \tag{6}$$

with the difference that in eq 6 the summation over j is performed over the discrete spectra of all ground-state vibrational frequencies j of the cluster; the values J_p and J_s are calculated now with the aid of the numerical values for the frequencies ω_j. Finally, in eq 6, Γ_p and θ_p are the homogeneous and inhomogeneous line width parameters on the transition s → p. The introduction of these parameters in the model gives the possibility to take into account the shape of the individual line and to avoid the appearance of discontinuities present in eq 4. In fact besides the values of the parameters Γ_p and θ_p, which are introduced in the program phenomenologically, ORCA[69,70,90] calculates all other parameters, which appear in eq 6, within the frames of DFT.[68] The total absorption coefficient is obtained by summation of all absorption bands arising on the transitions from the ground state to the excited ones. It should be mentioned that for the calculation of the energies of excited states the TDDFT method[91] is incorporated into the ORCA package.

5.2. Apparent Absorption Spectra of Bulk TiO_2 and Titania–Silica Model Clusters. At the first stage to test the calculation performance, the absorption spectrum of anatase was simulated. Reference calculations are based on the $Ti_9O_{30}H_{24}$ cluster (Figure 8), where the Ti_9O_{30} part reflects the crystal structure of the ideal bulk. For the TiO_2 compound the apparent absorption spectra have been measured in the present study using the polycrystalline powder material. In Figure 9 the calculated absorption spectra of the model $Ti_9O_{30}H_{24}$ cluster is compared with the experimental one of TiO_2. It is seen that the calculated spectrum reproduces quite

dx.doi.org/10.1021/jp504309w | J. Phys. Chem. C 2014, 118, 14677–14691

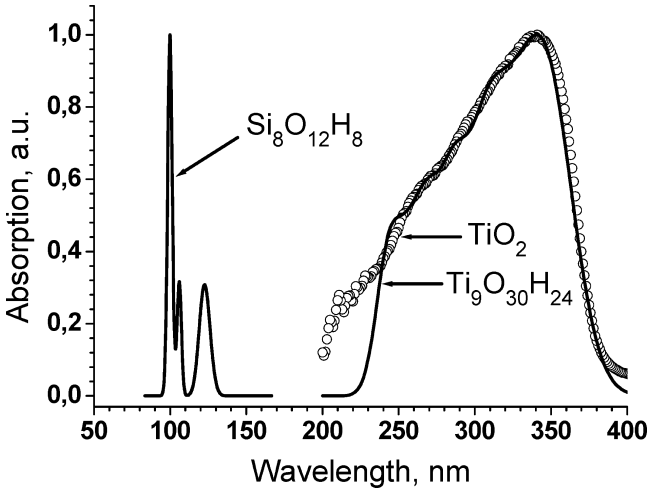

Figure 9. Observed apparent absorption spectra for TiO_2 bulk (circles) and calculated spectrum for the model $Ti_9O_{30}H_{24}$ cluster (solid line). The calculated spectrum of $Si_8O_{12}H_8$ cluster is shown for comparison.

well the features of the observed spectrum in a wide range of wavelengths 240−400 nm. Thus, the obtained results provide confidence that the calculated spectra of the VO_x, TiO_x, and TiO_x−VO_x species discussed below give reliable information. In the same figure the calculated apparent absorption spectra for the silsesquioxane $Si_8O_{12}H_8$ cluster (Figure 4) is shown. It is seen that the $Si_8O_{12}H_8$ species absorbs in the far ultraviolet range and does not influence the spectra of titania and vanadia samples.

In Figure 10 there are shown the calculated apparent absorption spectra of complexes $TiSi_7O_{13}H_8$ (a), $TiSi_7O_{14}H_{10}$ (b), $Ti_2Si_6O_{14}H_8$ (c), $Ti_2Si_{12}O_{23}H_{14}$ (g), $Ti_2Si_{14}O_{25}H_{14}$ (i) and the observed spectra for the samples 3Ti/SBA-15 and 8Ti/SBA-15. The notation of clusters corresponds to that in Figure 5. The difference in the calculated positions of the maxima of the bands presented in Figure 10 can be qualitatively explained as follows. It is seen that the maximum of the absorption curve for the cluster $TiSi_7O_{14}H_{10}$ (b) is blue shifted as compared to the maxima of the spectra arising from other clusters. This is probably connected with the presence of two OH ligands in the nearest environment of the single titanium ion in cluster (b), which requires a higher energy of ligand to metal electron transfer.

The close positions of the charge transfer bands for clusters $TiSi_7O_{13}H_8$ (a) and $Ti_2Si_{12}O_{23}H_{14}$ (g) probably originate from the similar environment of the titania ions in these clusters. The structure optimization shows that in clusters $Ti_2Si_6O_{14}H_8$ (c) and $Ti_2Si_{14}O_{25}H_{14}$ (i), the distance Ti−O−Ti is equal to 3.44 Å and 3.64 Å, respectively. Likely, this can lead to the red shifted band of cluster (c) since the transfer parameter p (see Figure 3a) is inversely proportional to the distance between the titanium ions.

At the same time the maxima of the curves corresponding to complexes $TiSi_7O_{13}H_8$ (a) and $Ti_2Si_{12}O_{23}H_{14}$ (g) are closer to that of the experimental one for 3Ti/SBA-15. These complexes may contribute to the spectra of 3Ti/SBA-15 and 8Ti/SBA-15 to some extent. The bands corresponding to clusters (b) and (i) are blue shifted relative to the observed ones, and the contribution of these clusters to the experimental curves is insignificant.

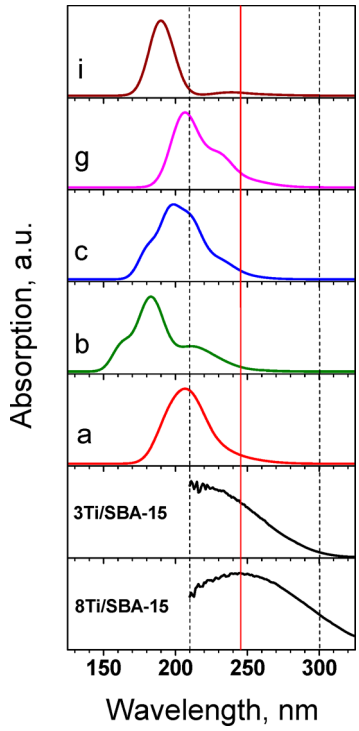

Figure 10. Calculated absorption spectra of clusters $TiSi_7O_{13}H_8$ (a), $TiSi_7O_{14}H_{10}$ (b), $Ti_2Si_6O_{14}H_8$ (c), $Ti_2Si_{12}O_{23}H_{14}$ (g), and $Ti_2Si_{14}O_{25}H_{14}$ (i) and the observed apparent absorption spectra for 3Ti/SBA-15 and 8Ti/SBA-15. The numeration of clusters corresponds to that in Figure 5.

A qualitatively different picture is presented in Figures 11a and 11b. It is seen that the spectra of the complexes $Ti_3Si_5O_{15}H_8$ (d), $Ti_4Si_4O_{16}H_8$ (f), $Ti_4Si_4O_{16}H_8$ (e), $Ti_8Si_8O_{31}H_{14}$ (j), and $Ti_3Si_{11}O_{24}H_{14}$ (h) may contribute significantly to the observed spectra of 3Ti/SBA-15 and 8Ti/

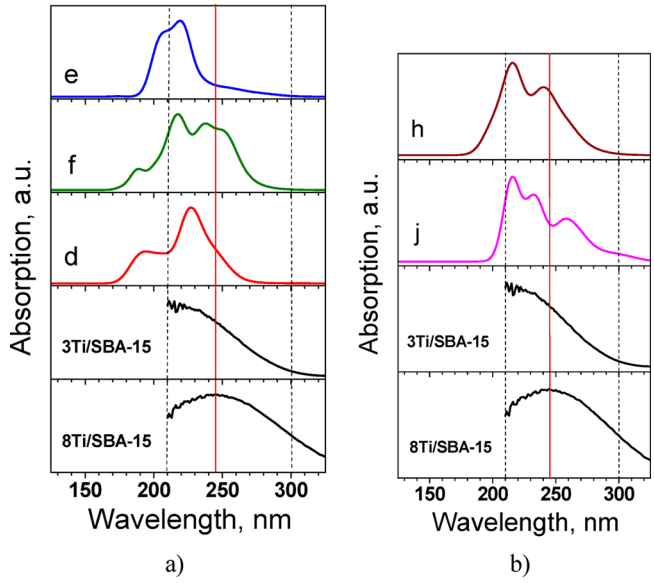

Figure 11. Calculated absorption spectra of clusters $Ti_3Si_5O_{15}H_8$ (d), $Ti_4Si_4O_{16}H_8$ (f), $Ti_4Si_4O_{16}H_8$ (e), $Ti_8Si_8O_{31}H_{14}$ (j), and $Ti_3Si_{11}O_{24}H_{14}$ (h) and the observed apparent absorption spectra for 3Ti/SBA-15 and 8Ti/SBA-15. The numeration of species corresponds to that in Figure 5.

dx.doi.org/10.1021/jp504309w | J. Phys. Chem. C 2014, 118, 14677−14691

SBA-15. In fact, the calculated spectra of the clusters $Ti_8Si_8O_{31}H_{14}$ (j) and $Ti_3Si_{11}O_{24}H_{14}$ (h) practically overlap with the experimental one for 3Ti/SBA-15 (Figure 12). The

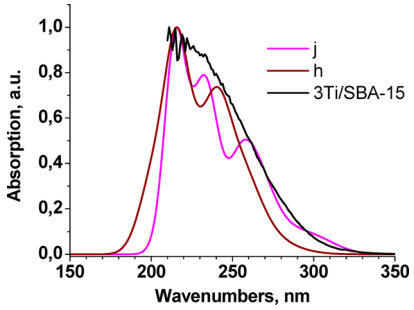

Figure 12. Calculated apparent absorption spectra of clusters $Ti_8Si_8O_{31}H_{14}$ (j) and $Ti_3Si_{11}O_{24}H_{14}$ (h) and the observed apparent absorption spectra for 3Ti/SBA-15.

contribution of cluster $Ti_4Si_4O_{16}H_8$ (f) to the spectra in the range 240 nm < λ < 270 nm is higher than for other clusters and exceeds the observed intensity for 3Ti/SBA-15. So, this more dense titanium oxide cluster most probably appears at loadings higher than 3 wt %. However, the examination performed leads to the conclusion that the formation of polynuclear titania clusters on the surface of SBA-15 is preferred already at low titanium oxide loadings. Isolated and binuclear titanium oxide species may contribute, but do not predominate.

5.3. Apparent Absorption Spectra of Vanadia–Silica Model Clusters. In Figures 13 and 14 the calculated apparent absorption spectra of vanadia clusters are shown together with the experimental ones for samples 1V/SBA-15 and 4V/SBA-15. The numeration of species corresponds to that in Figure 6. From Figure 13 it is seen that the first maximum of the charge transfer band corresponding to species (b) is blue shifted as

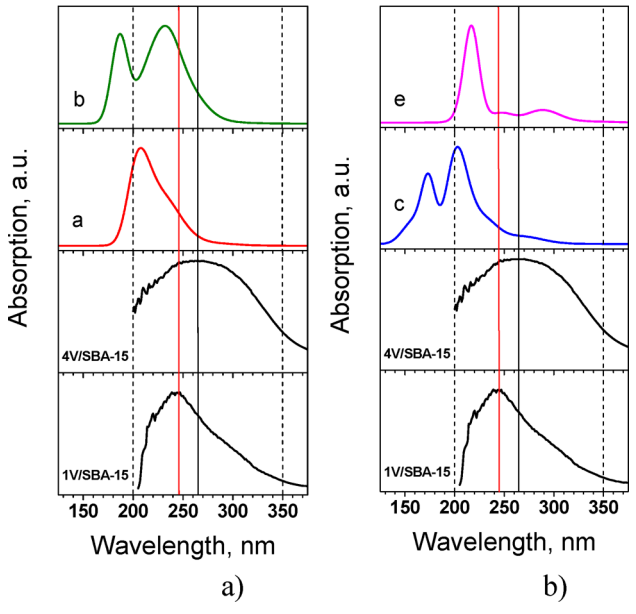

Figure 13. Calculated absorption spectra of species $VSi_7O_{13}H_7$ (a), $VSi_7O_{14}H_9$ (b), $VSi_7O_{15}H_{11}$ (c), $V_2Si_6O_{14}H_6$ (e) and the observed apparent absorption spectra for 1V/SBA-15 and 4V/SBA-15. The numeration of species corresponds to that in Figure 6.

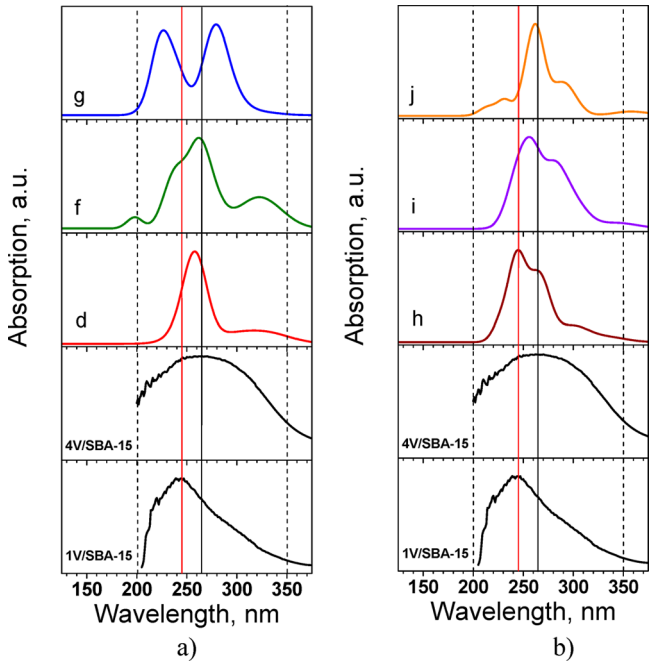

Figure 14. Calculated absorption spectra of species $VSi_7O_{15}H_9$ (d), $V_2Si_{12}O_{23}H_{12}$ (f), $V_2Si_{10}O_{20}H_{10}$ (g), $V_3Si_5O_{15}H_5$ (h), $V_3Si_{11}O_{24}H_{11}$ (i), and $V_4Si_4O_{16}H_4$ (j) and the observed apparent absorption spectra for 1V/SBA-15 and 4V/SBA-15. The numeration of species corresponds to that in Figure 6.

compared with that for species (a). Comparison of the experimental curves for 1V/SBA-15 and 4V/SBA-15 with the calculated one for species $VSi_7O_{14}H_9$ (b) shows that the latter may give a noticeable contribution to the spectra of 1V/SBA-15. The same species may also be present in 4V/SBA-15, which is in agreement with the experimental observation of V–OH groups in these samples.[42] The mononuclear species $VSi_7O_{15}H_{11}$ (c) and binuclear species $V_2Si_6O_{14}H_6$ (e) as it is seen from Figure 13b do not give appreciable contributions to the experimental spectra since the bands of these species are significantly shifted to the "blue" as compared with the observed peak positions. It is worth noting that species $VSi_7O_{15}H_9$ (d) and in particular the polynuclear vanadia species $V_2Si_{12}O_{23}H_{12}$ (f), $V_2Si_{10}O_{20}H_{10}$ (g), $V_3Si_5O_{15}H_5$ (h), $V_3Si_{11}O_{24}H_{11}$ (i), and $V_4Si_4O_{16}H_4$ (j) (Figure 14) may contribute to the spectra of 1V/SBA-15 as well as 4V/SBA-15. At the same time it is seen that the percentage of species $VSi_7O_{15}H_9$ (d), $V_2Si_{12}O_{23}H_{12}$ (f), and $V_2Si_{10}O_{20}H_{10}$ (g) in the spectra of 4V/SBA-15 should be appreciably higher than that in the spectra of 1V/SBA-15. One also cannot exclude the formation of species with higher nuclearity in 4V/SBA-15. Meanwhile, it is obvious that the degree of polymerization for vanadia deposited on the SBA-15 is generally lower than that for titania with similar loading.

5.4. Apparent Absorption Spectra of Vanadia–Titania–Silica Model Clusters. The $(VO_x)_n$–$(TiO_x)_n$/SBA-15 catalysts have been obtained in the following way. After covering the pore walls of SBA-15 with titania, vanadium oxide species have been subsequently grafted on the $(TiO_x)_n$/SBA-15 supports. On sub-monolayer TiO_x/SiO_2 catalysts, vanadia may be located on either, or both, of the titania and silica components (see ref 42 and references therein). Therefore, the V–Ti species selected for the calculations have been divided into three groups as described in section 4. In the

dx.doi.org/10.1021/jp504309w | J. Phys. Chem. C 2014, 118, 14677–14691

subsequent examination we do not consider the contribution of mononuclear or polynuclear species containing only V or Ti ions, which may be also present in mixed V−Ti catalysts. In this case the resulting spectra can be obtained by combination of spectra presented in Figures 9 and 10.

From Figure 15a it follows that in the group of mixed V−Ti species $TiVSi_6O_{14}H_7$ (a), $TiVSi_6O_{14}H_7$ (b), $TiVSi_{12}O_{23}H_{13}$ (c),

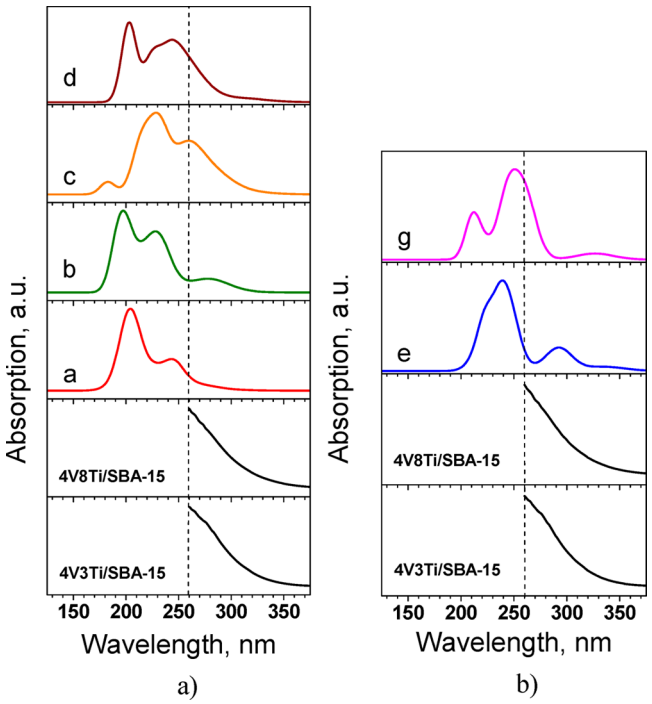

Figure 15. Calculated absorption spectra of species $TiVSi_6O_{14}H_7$ (a), $TiVSi_6O_{14}H_7$ (b), $TiVSi_{12}O_{23}H_{13}$ (c), $Ti_2VSi_{11}O_{24}H_{13}$ (d), $Ti_2V_2Si_4O_{16}H_6$ (e), and $Ti_2V_2Si_4O_{16}H_6$ (g) and the observed apparent absorption spectra for 4V3Ti/SBA-15 and 4V8Ti/SBA-15. The numeration of species corresponds to that in Figure 4.

and $Ti_2VSi_{11}O_{24}H_{13}$ (d), only species $TiVSi_{12}O_{23}H_{13}$ (c) may give a noticeable contribution to the spectra of the samples 4V3Ti/SBA-15 and 4V8Ti/SBA-15. However, this contribution cannot be considered as an appreciable one. Interestingly, species $Ti_2V_2Si_4O_{16}H_6$ (e) and $Ti_2V_2Si_4O_{16}H_6$ (g) (Figure 15b) containing similarities in the structure, namely, two neighboring V and two neighboring Ti ions with different mutual arrangement of the V−V and Ti−Ti pairs, give spectra with dominant contribution in the range of 200−290 nm. It should be mentioned also that the spectrum of species $Ti_4Si_4O_{16}H_8$ (e) has a small shoulder at 295 nm. Thus, it is seen that the contribution even of species $Ti_2V_2Si_4O_{16}H_6$ (e) to the spectrum intensity is insignificant. At the same time the bands arising from species $Ti_2V_2Si_4O_{16}H_6$ (f), $Ti_2V_2Si_4O_{16}H_6$ (h), and $Ti_3VSi_4O_{16}H_7$ (i) (Figure 16a) have shoulders of noticeable intensity in the range 250−320 nm and may contribute appreciably to the observed apparent absorption spectra. The common feature of these clusters is that they contain 4 alternating transition metal ions.

Clusters $Ti_4VSi_4O_{19}H_9$ (j), $Ti_4V_2Si_4O_{21}H_8$ (k), $Ti_4V_3Si_4O_{23}H_7$ (l), and $Ti_4V_4Si_4O_{24}H_4$ (m) (Figure 16b) with V ions anchored to titania contribute in a different way to the observed spectrum. The contribution of the cluster $Ti_4VSi_4O_{19}H_9$ (j) is in fact negligible. The spectrum of species $Ti_4V_2Si_4O_{21}H_8$ (k) with two titania anchored V ions is shifted

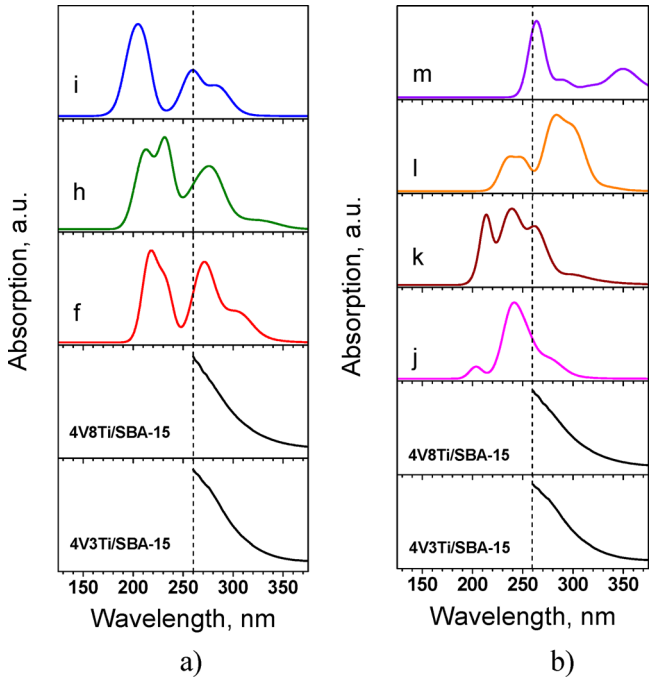

Figure 16. Calculated absorption spectra of species $Ti_2V_2Si_4O_{16}H_6$ (f), $Ti_2V_2Si_4O_{16}H_6$ (h), $Ti_3VSi_4O_{16}H_7$ (i), $Ti_4VSi_4O_{19}H_9$ (j), $Ti_4V_2Si_4O_{21}H_8$ (k), $Ti_4V_3Si_4O_{23}H_7$ (l), and $Ti_4V_4Si_4O_{24}H_4$ (m) and the observed apparent absorption spectra for 4V3Ti/SBA-15 and 4V8Ti/SBA-15. The numeration of species corresponds to that in Figure 4.

to the red as compared with the spectrum of $Ti_4VSi_4O_{19}H_9$ (j). However, it may contribute only in the range of 265−290 nm. Interestingly, species $Ti_4V_3Si_4O_{23}H_7$ (l) and $Ti_4V_4Si_4O_{24}H_4$ (m) apparently may contribute to spectra of catalysts with higher vanadia and titania loadings when the sublayer of Ti is covered almost completely by V ions. In summary, the performed calculations show that the spectra of the catalysts 4V3Ti/SBA-15 and 4V8Ti/SBA-15 may be formed by species of the type of $TiVSi_{12}O_{23}H_{13}$ (c), $Ti_2V_2Si_4O_{16}H_6$ (f), $Ti_2V_2Si_4O_{16}H_6$ (h), $Ti_3VSi_4O_{16}H_7$ (i) and small amounts of $Ti_4V_3Si_4O_{23}H_7$ (l), and $Ti_4V_4Si_4O_{24}H_4$ (m). Thus, the conclusion concerning the V−Ti catalysts is the following: The main contribution to the observed spectra comes from mixed V−Ti binuclear and tetranuclear species in which V and Ti ions are connected with each other and the support mainly through M−O−M (M = V, Ti) bridges, which are randomly distributed. Species that have only M−O−Si (M = V, Ti) bonds can be excluded. Accordingly, the majority of vanadia and titania species form a joint monolayer. Bilayer formation cannot be excluded but is not predominant. This is in agreement with experimental findings by infrared spectroscopy.[42]

6. CONCLUDING REMARKS

In the present communication we examined the UV−vis spectra of VO_x/SBA-15, TiO_x/SBA-15, and mixed $(VO_x)_n$−$(TiO_x)_n$/SBA-15 catalysts with the aim to reveal the underlying molecular structure of the surface oxide species. The motivation arises from the fact that the interpretation of UV−vis spectra of this type of catalyst in the literature is essentially based on qualitative examination and comparison with molecular or crystalline reference compounds. The composition of potential

dx.doi.org/10.1021/jp504309w | J. Phys. Chem. C 2014, 118, 14677−14691

surface species was taken from the literature as well as suggested by us from obvious considerations. For optimization of the structure of all chosen species and calculation of the apparent absorption spectra arising from these species the ORCA package[69,70] was applied. The reliability of the conclusions performed on the basis of DFT calculations within the ORCA package is supported by the nicely reproduced spectrum of TiO_2. The comparison of the observed spectra and those belonging to individual species gave a possibility to make a conclusion about the type of species present on the surface of the fresh catalyst after dehydration at elevated temperature. Generally, it becomes clear that not a single, well-defined species is present, but the spectra seem to reflect superimposed signals of a number of species, which is in agreement with the amorphous nature of the SBA-15 support.[92]

Titania species tend to polymerize on the surface of SBA-15 already at comparatively low titania loadings. Based on the present analysis it was found that on the surface of TiO_x/SBA-15 catalysts binuclear, trinuclear, tetranuclear, and even octanuclear titania clusters are present with high probability. Interestingly, the nuclearity of vanadia clusters at the surface of SBA-15 seems to be generally lower (mainly bi- and trinuclear, perhaps also tetranuclear) compared to the nuclearity of the corresponding titania clusters at comparable metal oxide loading. This is, in turn, reflected in a broader appearance of the absorption spectra of VO_x/SBA-15 compared to TiO_x/SBA-15. The results of the DFT calculations can be also supported by the following qualitative considerations. Since the oxidation degrees of vanadia and titania are +5 and +4, respectively, the band arising from charge transfer $O^{2-} \rightarrow Ti^{4+}$ in a single pair is blue shifted as compared with that in the pair $O^{2-} \rightarrow V^{5+}$ (Figure 3). At the same time the observed spectra for the catalysts 3Ti/SBA-15, 8Ti/SBA-15, 1V/SBA-15, and 4V/SBA-15 fall in the same range of wavelengths since the titania clusters contain a larger number of promoters.

According to our results, the nuclearity of vanadium oxide species increases with increasing loading, which is in agreement with qualitative interpretations discussed in the literature.[93] Isolated VO_x species, however, contribute only at the lowest vanadium oxide loading significantly to the absorption spectrum in the observable range, but only when the species bears a hydroxyl group. In the mixed $(VO_x)_n-(TiO_x)_n$/SBA-15 catalysts, the contributions to the spectra seem to be dominated by species that model a joint monolayer of titania and vandia species connected in a random way by M−O−Si (M = V, Ti) bonds. However, species that model a bilayer structure, which contain only V−O−Ti bonds, contribute as well.

In summary, the performed calculations clearly show that the simulation of the apparent absorption spectra can contribute to a better understanding of the molecular structure of surface oxide species in monolayer catalysts. Since UV−vis spectroscopy can also be performed under conditions of the catalytic reaction, the combination of experiment and theory can also deliver valuable information about the nature of the surface species in action on the surface of the working catalyst. The interpretation is, however, limited by experimental restrictions. Conventional UV−vis spectrometers allow measurements only at wavelengths $\lambda > 200$ nm, meanwhile, the calculated spectra of several species may reach into the range $\lambda < 200$ nm. This problem can be solved by performing the measurements in the absence of air in the optical path. Furthermore, independent calculations of infrared absorption and Raman spectra are necessary to quantify the contributions of different species, which will be addressed by us in future studies.

AUTHOR INFORMATION

Corresponding Author

*E-mail: klokishner@yahoo.com. Tel: (0037322)738604.

Notes

The authors declare no competing financial interest.

ACKNOWLEDGMENTS

The authors are grateful to Prof. B. S. Tsukerblat for fruitful discussion of the historical development of the theory of electron-vibrational bands. S.K. and O.R. are grateful to the Max-Planck Gesellschaft, Germany, for financial support. We thank T. Wolfram and D. Brennecke for synthesis of the catalysts. This work was supported by the German Research Foundation (Deutsche Forschungsgemeinschaft, DFG) through the cooperative research center "Structure, dynamics, and reactivity of transition metal oxide aggregates" (Sonderforschungsbereich 546, http://www.chemie.hu-berlin.de/sfb546).

REFERENCES

(1) Dunn, J. P.; Stenger, H. G., Jr.; Wachs, I. E. Oxidation of Sulfur Dioxide Over Supported Vanadia Catalysts: Molecular Structure−Reactivity Relationships and Reaction Kinetics. *Catal. Today* **1999**, *51*, 301−318.

(2) Dias, C. R.; Portela, M. F.; Bond, G. C. Synthesis of Phthalic Anhydride: Catalysts, Kinetics, and Reaction Modeling. *Catal. Rev.* **1997**, *39*, 169−207.

(3) Busca, G.; Lietti, L.; Ramis, G.; Berti, F. Chemical and Mechanistic Aspects of the Selective Catalytic Reduction of NO_x by Ammonia Over Oxide Catalysts: A review. *Appl. Catal., B* **1998**, *18*, 1−36.

(4) Blasco, T.; Lopez Nieto, J. M. Oxidative Dyhydrogenation of Short Chain Alkanes on Supported Vanadium Oxide Catalysts. *Appl. Catal., A* **1997**, *157*, 117−142.

(5) Yang, C.-C.; Vernimmen, J.; Meynen, V.; Cool, P.; Mul, G. Mechanistic Study of Hydrocarbon Formation in Photocatalytic CO_2 Reduction Over Ti-SBA-15. *J. Catal.* **2011**, *284*, 1−8.

(6) Brückner, A.; Rybarczyk, P.; Kosslick, H.; Wolf, G.-U.; Baerns, M. Highly Dispersed VO_x Species on Mesoporous Supports: Promising Catalysts for the Oxidative Dehydrogenation (ODH) of Propane. *Stud. Surf. Sci. Catal.* **2002**, *142*, 1141−1148.

(7) Burcham, L. J.; Deo, G.; Gao, X.; Wachs, I. E. In situ IR, Raman, and UV-Vis DRS Spectroscopy of Supported Vanadium Oxide Catalysts During Methanol Oxidation. *Top. Catal.* **2000**, *11/12*, 85−100.

(8) Das, N.; Eckert, H.; Hu, H.; Wachs, I. E.; Walzer, J. F.; Feher, F. J. Bonding States of Surface Vanadium(V) Oxide Phases on Silica: Structural Characterization by Vanadium-51 NMR and Raman Spectroscopy. *J. Phys. Chem.* **1993**, *97*, 8240−8243.

(9) Deo, G.; Turek, A. M.; Wachs, I. E.; Machej, T.; Haber, J.; Das, N.; Eckert, H.; Hirt, A. M. Physical and Chemical Characterization of Surface Vanadium Oxide Supported on Titania: Influence of the Titania Phase (Anatase, Rutile, Brookite and B). *Appl. Catal., A* **1992**, *91*, 27−42.

(10) Haber, J.; Nowak, P.; Serwicka, E. M.; Wachs, I. E. ESR Study of Monolayer Vanadium Oxide Catalysts Supported on Different Supports in Relation to Catalytic Oxidation of Methanol. *Bull. Polym. Acad. Sci. Chem.* **2000**, *48*, 337−346.

(11) Harlin, M. E.; Niemi, V. M.; Krause, A. O. I.; Weckhuysen, B. M. Effect of Mg and Zr Modification on the Activity of VOx/Al2O3 Catalysts in the Dehydrogenation of Butanes. *J. Catal.* **2001**, *203*, 242−252.

(12) Jhansi Lakshmi, L.; Ju, Z.; Alyea, E. C. Synthesis, Characterization, and Activity Studies of Vanadia Supported on Zirconia and Phosphorus-Modified Zirconia. *Langmuir* **1999**, *15*, 3521−3528.
(13) Lapina, O. B.; Khabibulin, D. F.; Shubin, A. A.; Bondareva, V. M. ^{51}V and ^{31}P NMR studies of VO_x/TiO_2 catalysts modified by phosphorous. *J. Mol. Catal. A* **2000**, *162*, 381−390.
(14) Olthof, B.; Khodakov, A.; Bell, A. T.; Iglesia, E. Effects of Support Composition and Pretreatment Conditions on the Structure of Vanadia Dispersed on SiO_2, Al_2O_3, TiO_2, ZrO_2, and HfO_2. *J. Phys. Chem. B* **2000**, *104*, 1516−1528.
(15) Ruitenbeck, M.; van Dillen, A. J.; de Groot, F. M. F.; Wachs, I. E.; Geus, J. W.; Konigsberger, D. C. The Structure of Vanadium Oxide Species on γ-Alumina; an in situ X-ray Absorption Study During Catalytic Oxidation. *Top. Catal.* **2000**, *10*, 241−254.
(16) Tanaka, T.; Yamashita, H.; Tsuchitani, R.; Funabiki, T.; Yoshida, S. X-ray Absorption (EXAFS/XANES) Study of Supported Vanadium Oxide Catalysts. Structure of Surface Vanadium Oxide Species On Silica and γ-Alumina at a Low Level of Vanadium Loading. *J. Chem. Soc., Faraday Trans.* **1988**, *84*, 2987−2999.
(17) Vurman, M. A.; Wachs, I. E. Raman Spectroscopy of V_2O_5, MoO_3, Fe_2O_3, MoO_3-V_2O_5, and Fe_2O_3-V_2O_5 Supported on Alumina Catalysts: Influence of Coverage and Dehydration. *J. Mol. Catal.* **1992**, *77*, 29−39.
(18) Wachs, I. E.; Chen, Y.; Jehnig, J.-M.; Briand, L. E.; Tanaka, T. Molecular structure and reactivity of the Group V metal oxides. *Catal. Today* **2003**, *78*, 13−24.
(19) Weckhuysen, B. M.; Keller, D. E. Chemistry, Spectroscopy and the Role of Supported Vanadium Oxides in Heterogeneous Catalysis. *Catal. Today* **2003**, *78*, 25−46.
(20) Stair, P. C. The Application of UV Raman Spectroscopy for the Characterization of Catalysts and Catalytic Reactions. In *Advances in Catalysis*; Gates, B. C., Knozinger, H., Eds.; Elsevier Academic Press Inc: San Diego, 2007; Vol. *51*, p 75.
(21) Kim, H.-S.; Stair, P. C. Resonance Raman Spectroscopic Study of Alumina-Supported Vanadium Oxide Catalysts with 220 and 287 nm Excitation. *J. Phys. Chem. A* **2009**, *113*, 4346−4355.
(22) Gao, X.; Bare, S. R.; Fierro, J. L. G.; Banares, M. A.; Wachs, I. E. Preparation and in-Situ Spectroscopic Characterization of Molecularly Dispersed Titanium Oxide on Silica. *J. Phys. Chem. B* **1998**, *102*, 5653−5666.
(23) Gao, X.; Wachs, I. E. Titania−Silica as Catalysts: Molecular Structural Characteristics and Physico-Chemical Properties. *Catal. Today* **1999**, *51*, 233−254.
(24) Perathoner, S.; Lanzafame, P.; Passalacqua, R.; Centi, G.; Schlögl, R.; Su, D. S. Use of Mesoporous SBA-15 for Nanostructuring Titania for Photocatalytic Applications. *Microporous Mesoporous Mater.* **2006**, *90*, 347−361.
(25) Cozzolino, M.; Di Serio, M.; Tesser, R.; Santacesaria, E. Grafting of Titanium Alkoxides on High-Surface SiO_2 Support: An Advanced Technique for the Preparation of Nanostructured TiO_2/SiO_2 Catalysts. *Appl. Catal., A* **2007**, *325*, 256−362.
(26) Zukerman, R.; Vradman, L.; Titelman, L.; Weidenthaler, C.; Landau, M. V.; Herskowitz, M. Effect of Silica Wall Microporosity on the State and Performance of TiO_2 Nanocrystals in SBA-15 Matrix. *Microporous Mesoporous Mater.* **2008**, *116*, 237−245.
(27) Lu, J.; Kosuda, K. M.; Van Duyne, R. P.; Stair, P. C. Surface Acidity and Properties of TiO_2/SiO_2 Catalysts Prepared by Atomic Layer Deposition: UV−visible Diffuse Reflectance, DRIFTS, and Visible Raman Spectroscopy Studies. *J. Phys. Chem. C* **2009**, *113*, 12412−12418.
(28) Zhang, F.; Carrier, X.; Krafft, J.-M.; Yoshimura, Y.; Blanchard, J. Insight Into the Structure and Localization of the Titania Overlayer in TiO_2-Coated SBA-15 Materials. *New J. Chem.* **2010**, *34*, 508−516.
(29) Guo, C. S.; Hermann, K.; Hävecker, M.; Trunschke, A.; Schlögl, R. Silica-Supported Titania Species: Structural Analysis from Quantum Theory and X-ray Spectroscopy. *J. Phys. Chem. C* **2012**, *116*, 22449−22457.
(30) Wachs, I. E. Recent Conceptual Advances in the Catalysis Science of Mixed Metal Oxide Catalytic Materials. *Catal. Today* **2005**, *100*, 79−94.
(31) Wachs. I. E. Molecular Structures of Surface Metal Oxide Species: Nature of Catalytic Active Sites in Mixed Metal Oxides. In *Metal Oxides: Chemistry and Applications*; Fierro, J. L. G., Heinemann, H., Eds.; CRC Taylor & Francis Press: Boca Raton, FL, 2005; pp 1−30.
(32) Khodakov, A.; Olthof, B.; Bell, A. T.; Iglesia, E. Structure and Catalytic Properties of Supported Vanadium Oxides: Support Effects on Oxidative Dehydrogenation Reactions. *J. Catal.* **1999**, *181*, 205−216.
(33) Bond, G. C.; Flamerz-Tahir, S. Vanadium Oxide Monolayer Catalysts Preparation, Characterization and Catalytic Activity. *Appl. Catal.* **1991**, *71*, 1−31.
(34) Deo, G.; Wachs, I. E.; Haber, J. Supported Vanadium Oxide Catalysts: Molecular Structural Characterization and Reactivity Properties. *Crit. Rev. Surf. Chem.* **1994**, *4*, 141−187.
(35) Wachs, I. E.; Weckhuysen, B. M. Structure and Reactivity of Surface Vanadium Oxide Species on Oxide Supports. *Appl. Catal., A* **1997**, *157*, 67−90.
(36) Muylaert, I.; Van Der Voort, P. Supported Vanadium Oxide in Heterogeneous Catalysis: Elucidating the Structure−Activity Relationship with Spectroscopy. *Phys. Chem. Chem. Phys.* **2009**, *11*, 2826−2832.
(37) Hess, C. Nanostructured Vanadium Oxide Model Catalysts for Selective Oxidation Reactions. *ChemPhysChem* **2009**, *10*, 319−326.
(38) Zhao, D.; Feng, J.; Huo, Q.; Melosh, N.; Fredrickson, G. H.; Chmelka, B. F.; Stucky, G. D. Triblock Copolymer Syntheses of Mesoporous Silica with Periodic 50 to 300 Angstrom Pores. *Science* **1998**, *279*, 548−552.
(39) Zhao, D.; Huo, Q.; Feng, J.; Chmelka, B. F.; Stucky, G. D. Nonionic Triblock and Star Diblock Copolymer and Oligomeric Surfactant Syntheses of Highly Ordered, Hydrothermally Stable, Mesoporous Silica Structures. *J. Am. Chem. Soc.* **1998**, *120*, 6024−6036.
(40) Liu, Y. M.; Cao, Y.; Yi, N.; Feng, W. L.; Dai, W. L.; Yan, S. R.; He, H. Y.; Fan, K. N. Vanadium Oxide Supported on Mesoporous SBA-15 as Highly Selective Catalysts in the Oxidative Dehydrogenation of Propane. *J. Catal.* **2004**, *224*, 417−428.
(41) Gruene, P.; Wolfram, T.; Pelzer, K.; Schlögl, R.; Trunschke, A. Role of Dispersion of Vanadia on SBA-15 in the Oxidative Dehydrogenation of Propane. *Catal. Today* **2010**, *157*, 137−142.
(42) Hamilton, N.; Wolfram, T.; Tzolova-Müller, G.; Hävecker, M.; Kröhnert, J.; Carrero, C.; Schomäcker, R.; Trunschke, A.; Schlögl, R. Topology of Silica Supported Vanadium−Titanium Oxide Catalysts for Oxidative Dehydrogenation of Propane. *Catal. Sci. Technol.* **2012**, *2*, 1346−1359.
(43) Van Lingen, J. N. J.; Gijzeman, O. L. J.; Havenith, R. W. A.; van Lenthe, J. H. Determining the Structure of Silica-Supported Monomeric Vanadium Oxide Catalysts Based on Synthesis Method and Spectral Data from Theoretical Calculations. *J. Phys. Chem. C* **2007**, *111*, 7071−7077.
(44) Anpo, M.; Sunamoto, M.; Che, M. Preparation of Highly Dispersed Anchored Vanadium Oxides by Photochemical Vapor Deposition Method and Their Photocatalytic Activity for Isomerization of Trans-2-Butene. *J. Phys. Chem.* **1989**, *93*, 1187−1189.
(45) Bond, G. C.; König, P. The Vanadium Pentoxide-Titanium Dioxide System: Part 2. Oxidation of o-Xylene on a Monolayer Catalyst. *J. Catal.* **1982**, *77*, 309−322.
(46) Deo, G.; Wachs, I. E. Surface Oxide-Support Interaction (SOSI) for Surface Redox Sites. *J. Catal.* **1991**, *129*, 307−312.
(47) Hardcastle, F. D.; Wachs, I. E. Determination of Vanadium-Oxygen Bond Distances and Bond Orders by Raman Spectroscopy. *J. Phys. Chem.* **1991**, *95*, 5031−5041.
(48) Lee, E. L.; Wachs, I. E. In Situ Raman Spectroscopy of SiO_2-Supported Transition Metal Oxide Catalysts: An Isotopic $^{18}O-^{16}O$ Exchange Study. *J. Phys. Chem. C* **2008**, *112*, 6487−6498.

(49) Weckhuysen, B. M.; Jehnig, J. M.; Wachs, I. E. In Situ Raman Spectroscopy of Supported Transition Metal Oxide Catalysts: $^{18}O_2$–$^{16}O_2$ Isotopic Labeling Studies. *J. Phys. Chem. B* **2000**, *104*, 7382–7387.
(50) Went, G. T.; Oyama, S. T.; Bell, A. T. Laser Raman Spectroscopy of Supported Vanadium Oxide Catalysts. *J. Phys. Chem.* **1990**, *94*, 4240–4246.
(51) Bond, G. C.; Perez Zurita, J.; Flamerz, S.; Gellings, P. J.; Bosch, H.; Van Ommen, J. G.; Kip, B. J. Structure and Reactivity of Titania-Supported Oxides. Part 1: Vanadium Oxide on Titania in the Sub- and Super-Monolayer Regions. *J. Appl. Catal.* **1986**, *22*, 361–378.
(52) Deguns, E. W.; Taha, Z.; Meitzner, G. D.; Scott, S. L. An X-ray Absorption Study of Two $VOCl_3$-Modified Silicas: Evidence for Chloride–Silica Interactions. *J. Phys. Chem. B* **2005**, *109*, 5005–5011.
(53) Ferreira, M. L.; Volpe, M. On the Nature of Highly Dispersed Vanadium Oxide Catalysts: Effect of the Support on the Structure of VO_x Species. *J. Mol. Catal. A* **2000**, *164*, 281–290.
(54) Khaliulin, R. Z.; Bell, A. T. A Density Functional Theory Study of the Oxidation of Methanol to Formaldehyde over Vanadia Supported on Silica, Titania, and Zirconia. *J. Phys. Chem. B* **2002**, *106*, 7832–7838.
(55) Vittadina, A.; Selloni, A. Periodic Density Functional Theory Studies of Vanadia–Titania Catalysts: Structure and Stability of the Oxidized Monolayer. *J. Phys. Chem. B* **2004**, *108*, 7337–7343.
(56) Keller, D. E.; de Groot, F. M. F.; Koningsberger, D. C.; Weckhuysen, B. M. ΛO4 Upside Down:A New Molecular Structure for Supported VO_4 Catalysts. *J. Phys. Chem. B* **2005**, *109*, 10223–10233.
(57) Gijzeman, O. L. J.; Van Lingen, J. N. J.; Van Lenthe, J. H.; Tinnemans, S. J.; Keller, D. E.; Weckhuysen, B. M. A New Model for the Molecular Structure of Supported Vanadium Oxide Catalysts. *Chem. Phys. Lett.* **2004**, *397*, 277–281.
(58) Van Lingen, J. N. J.; Gijzeman, O. L. J.; Van Lenthe, J. H.; Weckhuysen, B. M. On the Umbrella Model for Supported Vanadium Oxide Catalysts. *J. Catal.* **2006**, *239*, 34–41.
(59) Keller, D. E.; Koningsberger, D. C.; Weckhuysen, B. Molecular Structure of a Supported VO_4 Cluster and Its Interfacial Geometry as a Function of the SiO_2, Nb_2O_5, and ZrO_2 Support. *J. Phys. Chem. B* **2006**, *110*, 14313–14325.
(60) Hävecker, M.; Cavalleri, M.; Herbert, R.; Follath, R.; Knop-Gericke, A.; Hess, C.; Hermann, K.; Schlögl, R. Methodology for the Structural Characterisation of V_xO_y Species Supported on Silica Under Reaction Conditions by Means of in Situ O K-edge X-ray Absorption Spectroscopy. *Phys. Status Solidi B* **2009**, *246*, 1459–1469.
(61) Cavalleri, M.; Hermann, K.; Knop-Gericke, A.; Hävecker, M.; Herbert, R.; Hess, C.; Oestereich, A.; Döbler, J.; Schlögl, R. Analysis of Silica-Supported Vanadia by X-ray Absorption Spectroscopy: Combined Theoretical and Experimental Studies. *J. Catal.* **2009**, *262*, 215–223.
(62) Kim, H.-S.; Zygmunt, S. A.; Stair, P. C.; Zapol, P.; Curtiss, L. A. Monomeric Vanadium Oxide on a θ-Al_2O_3 Support: A Combined Experimental/Theoretical Study. *J. Phys. Chem. C* **2009**, *113*, 8836–8843.
(63) Wu, Z.; Dai, S.; Overbury, S. H. Multiwavelength Raman Spectroscopic Study of Silica-Supported Vanadium Oxide Catalysts. *J. Phys. Chem. C* **2010**, *114*, 412–422.
(64) Kobayashi, H.; Yamaguchi, M.; Tanaka, T.; Yoshida, S. Ab Initio Molecular-Orbital Study on the Adsorption of Ethylene and Oxygen Molecules Over Vanadium Oxide Clusters. *J. Chem. Soc., Faraday Trans. 1* **1985**, *81*, 1513–1525.
(65) Takenaka, S.; Tanaka, T.; Yamazaki, T.; Funabiki, T.; Yoshida, S. Structure of Active Species in Alkali-Ion-Modified Silica-Supported Vanadium Oxide. *J. Phys. Chem. B* **1997**, *101*, 9035–9040.
(66) Magg, N.; Immarapon, B.; Giorgi, J. B.; Schroeder, T.; Bäumer, M.; Döbler, J.; Wu, Z.; Kondratenko, E.; Cherian, M.; Baerns, M.; Stair, P. C.; Sauer, J.; Freund, H.-J. Vibrational Spectra of Alumina- and Silica-Supported Vanadia Revisited: An Experimental and Theoretical Model Catalyst Study. *J. Catal.* **2004**, *226*, 88–100.
(67) Döbler, J.; Pritzsche, M.; Sauer, J. Vibrations of Silica Supported Vanadia: Variation with Particle Size and Local Surface Structure. *J. Phys. Chem. C* **2009**, *113*, 12454–12464.
(68) Parr, R. G.; Yang, W. *Density-Functional Theory of Atoms and Molecules*; Oxford University Press: New York, 1989.
(69) Neese, F. Prediction of Molecular Properties and Molecular Spectroscopy with Density Functional Theory: From Fundamental Theory to Exchange-Coupling. *Coord. Chem. Rev.* **2009**, *253*, 526–563.
(70) Neese F.; et al. *ORCA, an ab initio, DFT and semiempirical SCF-MO package, Version 2.8–20 September 2010*; Lehrstuhl für Theoretische Chemie: Wegelstrasse, 12D-531115 Bohn, Germany.
(71) Zhang, Y.; Yang, W. A Comment on the Letter by John P. Perdew, Kieron Burke, and Matthias Ernzerhof. *Phys. Rev. Lett.* **1998**, *80*, 890.
(72) Matveev, A. A.; Staufer, M.; Mayer, M.; Rösch, N. Density Functional Study of Small Molecules and Transition-Metal Carbonyls Using Revised PBE Functionals. *Int. J. Quantum Chem.* **1999**, *75*, 863–873.
(73) Deeth, R. J.; Fey, N. J. The Performance of Nonhybrid Density Functionals for Calculating the Structures and Spin States of Fe(II) and Fe(III) Complexes. *Comput. Chem.* **2004**, *25*, 1840–1848.
(74) Zein, S.; Borshch, S. A.; Fleurat-Lessard, P.; Casida, M. E.; Chemette, H. Assessment of the Exchange-Correlation Functionals for the Physical Description of Spin Transition Phenomena by Density Functional Theory Methods: All the Same? *J. Chem. Phys.* **2007**, *126*, 014105.
(75) Kuta, J.; Patchkovskii, S.; Zgierski, M. Z.; Kozlowski, P. M. Performance of DFT in Modeling Electronic and Structural Properties of Cobalamins. *J. Comput. Chem.* **2006**, *27*, 1429–1437.
(76) Fajín, J. L. C.; Illas, F.; Gomes, J. R. B. Effect of the Exchange-Correlation Potential and of Surface Relaxation on the Description of the H_2O Dissociation on Cu(111). *J. Chem. Phys.* **2009**, *130*, 224702.
(77) Roldán, A.; Ricart, J. M.; Illas, F. Influence of the Exchange–Correlation Potential on the Description of the Molecular Mechanism of Oxygen Dissociation by Au Nanoparticles. *Theor. Chem. Acc.* **2009**, *123*, 119–126.
(78) Schaefer, A.; Horn, H.; Ahlrichs, R. Fully Optimized Contracted Gaussian Basis Sets for Atoms Li to Kr. *J. Chem. Phys.* **1992**, *97*, 2571–2577.
(79) Weigend, F.; Ahlrichs, R. Balanced Basis Sets of Split Valence, Triple Zeta Valence and Quadruple Zeta Valence Quality for H to Rn: Design and Assessment of Accuracy. *Phys. Chem. Chem. Phys.* **2005**, *7*, 3297–3305.
(80) Kossmann, S.; Neese, F. Efficient Structure Optimization with Second-Order Many-Body Perturbation Theory: The RIJCOSX-MP2 Method. *J. Chem. Theory Comput.* **2010**, *6*, 2325–2338.
(81) Feher, F. J.; Walzer, J. F. Synthesis and Characterization of Vanadium-Containing Silsesquioxanes. *Inorg. Chem.* **1991**, *30*, 1689–1694.
(82) Pekar, S. I. Theory of F-Centers. *Sov. Phys.—JETP* **1950**, *20*, 510–522.
(83) Huang, K.; Rhys, A. Theory of Light Absorption and Non-Radiative Transitions in F-Centres. *Proc. R. Soc.* **1950**, *A204*, 406–423.
(84) Markham, J. J. Interaction of Normal Modes with Electron Traps. *Rev. Mod. Phys.* **1959**, *31*, 956–989.
(85) Krivoglaz, M. A.; Pekar, S. I. Shape of Impurity Absorption and Luminescence Spectra in Dielectrics. *Proc. Inst. Phys. AN USSR* **1953**, *4*, 37–70.
(86) Kubo, R.; Toyazawa, Y. Application of the Method of Generating Function to Radiative and Non-Radiative Transitions of a Trapped Electron in a Crystal. *Prog. Theor. Phys.* **1955**, *13*, 160–182.
(87) Perlin, Yu. E. Modern Methods in the Theory of Many-Phonon Processes. *Sov. Phys.—Usp.* **1963**, *80*, 553.
(88) Perlin, Yu. E.; Tsukerblat, B. S. Optical Bands and Polarization Dichroism of Jahn-Teller Centers. In *The dynamical Jahn-Teller effect in localized systems*; Perlin, Yu. E., Wagner, M., Eds.; Elsevier: Amsterdam, 1984; Vol. 7.

(89) Perlin, Yu. E.; Tsukerblat, B. S. Effects of Electron-Vibrational Interactionin in the Optical Spectra of Impurity Ions, Ştiinţa, Kishinev. **1974**

(90) Petrenko, T.; Krylova, O.; Neese, F.; Sokolowski, M. Optical Absorption and Emission Properties of Rubrene: Iinsight From a Combined Experimental and Theoretical Study. *New J. Phys.* **2009**, *11*, 015001.

(91) Runge, E.; Gross, E. K. U. Density-Functional Theory for Time-Dependent Systems. *Phys. Rev. Lett.* **1984**, *52*, 997−1000.

(92) Amakawa, K.; Sun, L.; Guo, C.; Hävecker, M.; Kube, P.; Wachs, I. E.; Lwin, S.; Frenkel, A. I.; Patlolla, A.; Hermann, K.; A.; et al. How Strain Affects the Reactivity of Surface Metal Oxide Catalysts. *Angew. Chem., Int. Ed.* **2013**, *52*, 13553−13557.

(93) Gao, X.; Wachs, I. E. Investigation of Surface Structures of Supported Vanadium Oxide Catalysts by UV−vis−NIR Diffuse Reflectance Spectroscopy. *J. Phys. Chem. B* **2000**, *104*, 1261−1268.